University of Bremen

Alfred Wegener Institute, Helmholtz Centre for Polar and Marine Research

Master's Thesis

Cretaceous Simulation with the Earth System Model AWI-ESM-2

Author:

Gidado Kowiy Tunde

Matriculation Number:

3121376

First Supervisor:

Prof. Dr. Gerrit Lohmann

Second Supervisor:

Dr. Johann Klages

Tutor(s):

Dr. Gregor Knorr

Dr. Paul Gierz

December, 2021

Declaration of Copyright

I hereby declare, that this master thesis was written without external support and that no sources and auxiliary means other than those quoted were used. All statements analogously or literally copied from other publications have been identified as quotations.

In addition, I authorize that this thesis report be made available on the University of Bremen research archive.

Bremen / December, 2021 Kowiy Tunde Gidado

Abstract

The Earth's climate during the Cretaceous period was characterized by temperatures warmer than today driven by a high CO_2 level. Due to the continuous rise in our atmospheric CO_2 concentration since the Industrial Revolution, Cretaceous climate is now of particular interest as a suitable analog to our future climate changes. Here, the Cretaceous climate has been investigated using the newly developed AWI-Earth System Model 2(AWI-ESM-2) with interactive vegetation at different CO_2 concentrations. The AWI-ESM-2 employs coupled sub-models of FESOM with unstructured mesh, the ECHAM running on T63 grid and a land surface scheme with interactive vegetation dynamics to produce a reasonable representation of Cretaceous climate and vegetation. The atmospheric CO_2 concentrations of 1x, 4x, 6x the PI value (280ppm) with other greenhouse gases (N_2O and CH_4) fixed at PI levels were used to run three modeling experiments.

Results obtained indicated a warmer surface temperature and vanishing of sea ice cover at the two higher CO_2 experiments, with the Antarctic summer temperature as warm as 23 ^oC and a completely ice free Antarctic continent at the CR_6x simulation. At both CR_4x and CR_6x simulations, snow presence was seasonally dependent, with upto 25cm snow present in the high latitudes at both Austral and Boreal winter, indicating seasonal dependency. The tropics were generally wetter, most especially the summer of CR_6x, while the precipitation level of Antarctica appears similar. Also, the Antarctic mid-Cretaceous terrestrial ecosystem seems to be sensitive to CO_2 changes, as the coniferous evergreen forest dominated continent during the CR_1x simulation shifted to a mix of coniferous and extra-tropical evergreen trees under both CR_4x and CR_6x. Additionally, comparing PI and mid-Cretaceous simulations at 280 ppmv and 1120 ppmv shows that CR_4x has an average surface temperature much warmer than PI_4x, especially towards the South Pole.

These findings are consistent with the idea that a temperate climate in the high latitude of mid-Cretaceous period requires high CO_2 forcing and that permanent ice cannot survive towards the South Pole with an elevated CO_2. The interactive vegetation approach also confirms the influence of important feedbacks particularly over ice free Antarctica.

ACKNOWLEDGEMENTS

Firstly, I would like to thank my first supervisor Prof. Dr. Gerrit Lohmann for accepting me into the Paleoclimate Dynamics section at Alfred Wegener Institute (AWI) Bremerhaven, to undertake my master thesis. I appreciate his support and great encouragement throughout the study period. Many thanks to my second supervisor, Dr. Johann Phillip Klages for providing this astonishing idea and the background leading to this study.

My utmost appreciation goes to Dr. Paul Gierz and Dr. Gregor Knorr for their motivation and tutelage. I have greatly benefited from their wealth of knowledge and experiences. Their mentorship was perfect for executing such a daunting research work.

Finally, I thank my family members and everyone else who has contributed to my academic accomplishments. God bless you all.

Contents

CHAPTER 1

Introduction

The Cretaceous period was the final period of the Mesozoic era, covering about 80Ma (144 – 66Ma, where Ma represents million years before the present date). The climate of this period was much warmer than today, with proofs suggesting that mean annual temperatures were 7 – 14 degrees Celsius (°C) warmer than present (Francis et al, 2007; Poole et al, 2005; Otto-Bliesner et al, 2002) and atmospheric carbon dioxide (CO_2) concentrations were 2 to 10 times greater than today (e.g Berner, 1997; Klages et al., 2020). This was termed a *"greenhouse climate"*, which resulted in a less varying climate system with lower cycles of seasonal temperature as well as polar temperature above freezing point, thus leading to a lower equator-to-pole temperature gradient (Barron, 1983; Sloan & Barron, 1990; Valdes et al, 1996). Based on proxy records, no significant ice sheet may have existed in this period and the sea level was about 170 meters higher than today (Miller et al, 2005; Muller et al, 2008; Klages et al., 2020).

Anthropogenic activities in the last two centuries have resulted in a rising level of atmospheric CO_2 concentration, a level currently higher than the 300 parts per million by volume (ppmvv) maximum (based on measurement of air in ice cores) ever recorded in the 800 kiloyears (ka) before the industrial revolution. There is currently about 416ppmv atmospheric CO_2, 48% more than the ~280 ppmvv in the year 1750, leading to a global temperature rise of about 1°C in the last 100 years. Despite the difference in the present day and the Cretaceous boundary conditions and paleogeography, the increasing atmospheric CO_2 concentrations has fueled interests in the significance of understanding the Cretaceous climate, due to the possibility of the Cretaceous greenhouse conditions reappearing in the near future (Hay, 2011).

Coupled atmosphere-ocean General Circulation Models (GCMs) are frequently employed to

simulate the past and present climates, thereby helping us improve our understanding of the global climate system and offering significant use to our society due to the accelerating impacts of climate change (Karl & Trenberth, 2003). The coupled atmosphere-ocean GCM is a simplified numerical model of climate system in a global grid which integrates complex exchanges between various climate system components in the simulation of paleoclimate, present climate and future climate projections (Reichler et al, 2008), and most importantly under different greenhouse gas forcing.

Modelling complex systems means GCMs are prone to model biases. Therefore, there is sometimes the need for comparison between observational data and other models in a model assemblage simulation (Edwards, 2011). Increasing complexity and resolution advancement of climate models has led to the rise of Coupled Earth System Models (ESMs) and more interests in Integrated Assessment Models (IAMs) that include additional components to the models (Hannah, 2015). In this framework, the AWI Earth System Model has been used for the paleoclimate simulation presented here.

1.2 Cretaceous timescale

The Cretaceous is divided into two epochs, the early (145 - 100.5 Ma) and late Cretaceous (100.5 - 66Ma), which are again subdivided into twelve stages as outlined in Figure 1.1. At the beginning of the Cretaceous only two large continents were present on earth, *Gondwana* in the Southern Hemisphere and *Laurasia* in the Northern Hemisphere, which were largely separated by the equatorial Tethys seaway. However, towards the end of the Cretaceous, there was an accelerated fragmentation of those continents, slowly developing towards the modern configuration.

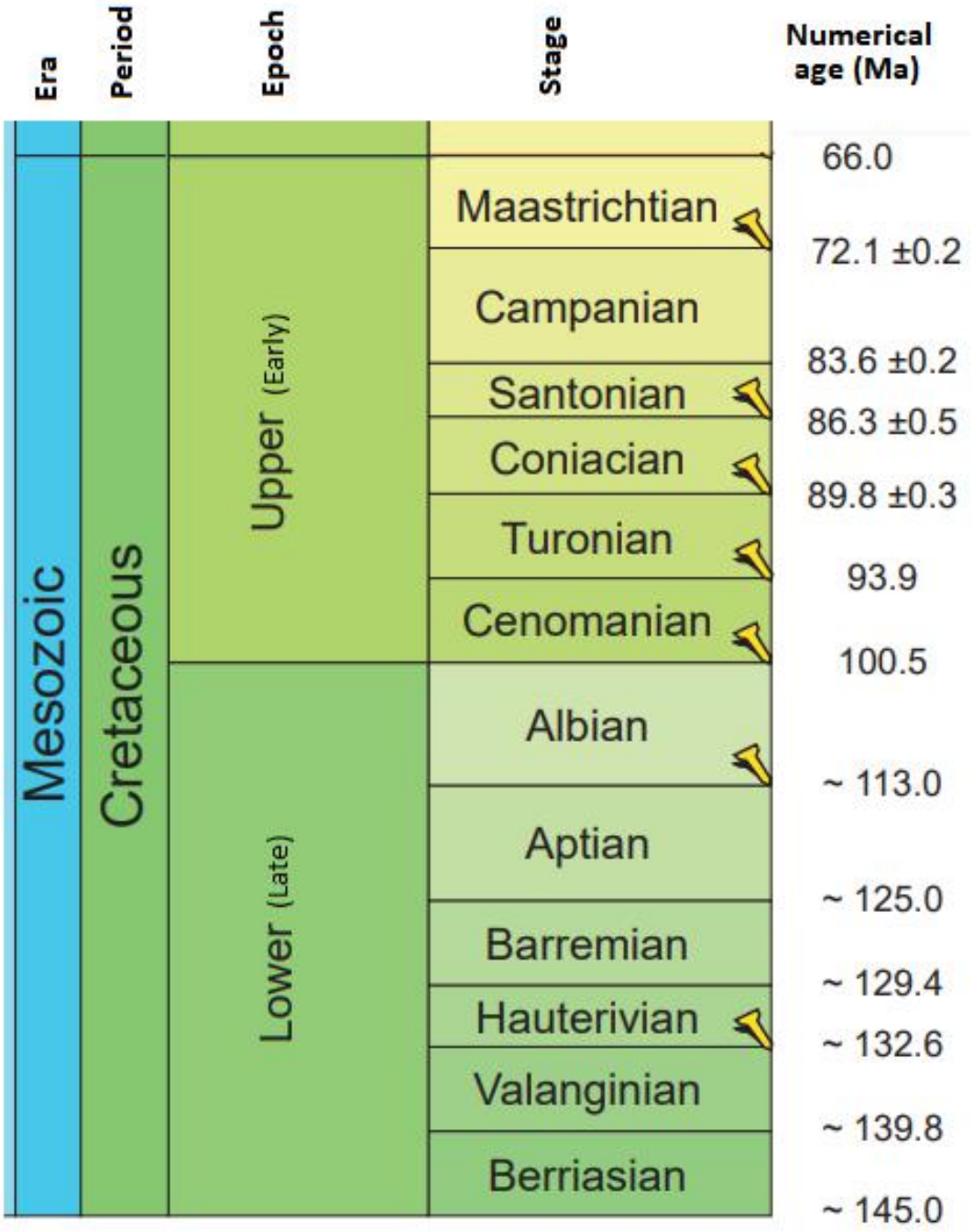

Figure 1.1: Geological timescale showing the Cretaceous Period (https://stratigraphy.org/ICSchart/ChronostratChart2021-10.pdf)

During the Cretaceous, total land area was about 20% less than today, especially in the Northern Hemisphere. As a result, land-sea distribution has been suggested by initial GCM simulations as a possible reason for the Cretaceous warmth due to discrete land-sea thermal attributes (Barron & Washington, 1984). These GCM experiments employs yearly mean climate models with facile energy balance ocean that fails to estimate seasonal changes in insulation, thereby inhibiting high latitude continental seasonal cycle. However, a similar influence of Cretaceous paleogeography in relation to high atmospheric CO_2 forcing was proven by other GCM simulations that employed seasonally varying insulation with a 50m slab ocean model, capturing the seasonal thermal cycle of the ocean mixed layer (DeConto et al., 2000). Nonetheless, regional paleogeography is highly significant in paleoclimate simulation due to their contribution to warmer land area next to inland seas of the Eocene and mid-Cretaceous (Valdes et al., 1996).

1.3 Background study

Otto-Bliesner et al. (2002) simulated the late Cretaceous ocean using the National Centre for Atmospheric Research Climate System Model (NCAR CSM). The NCAR CSM is a coupled atmosphere-ocean-sea ice- land surface model (Otto-Bliesner & Brandy, 2001). They ran an atmosphere and land model for 20 years which was used as initial and boundary conditions and forcing to the ocean/sea ice spin up, integrated for another 100 years. Both spin ups were used to initialize a fully coupled atmosphere-land-ocean-sea-ice simulation with increased CO_2 (1680ppmv) integrated for 130years. A comparison of the observed results to a present simulation with current geography, bathymetry and solar constant, suggests that the surface ocean, temperature, salinity and circulation was undoubtedly disparate. The deep water formation of the Cretaceous also differs from the present, with sinking in North Pacific due to cooling of the warmer and saltier water.

Niezgodzki et al. (2017) modelled the latest Cretaceous climate using the Earth System Model COSMOS. The model was forced with different CO_2 levels to obtain surface temperatures which were compared to corresponding proxy-based temperature reconstructions. They observed the most feasible match with the proxy data for

temperatures simulated with 3 to 5 times PI CO_2 level, but there is less correspondence between the modelled surface temperature and the proxy data on a regional scale.

Higuchi et al. (2021) compared the difference between Present day and mid-Cretaceous hydrological cycles by simulating a Cretaceous climate with varied CO_2 levels in an atmosphere-ocean GCM, they compared the experiments with a present day simulation and proxy data of the Cretaceous world. A decrease in East Asia low latitude rainfall was found during the Cretaceous run, a finding coherent with geological data on mid-Cretaceous hydrology. On the other hand, the same region experienced an increased rainfall under the present-day simulation. This reversal was attributed to summer atmospheric circulation due to exclusion of Tibetan Plateau in the Cretaceous period, therefore showing the significance of background geographical conditions on climate warming inducing changes of the regional water cycle.

The structure and function of the Earth ecosystem is affected by atmospheric inputs while the features of the terrestrial ecosystem (leaf area index, canopy roughness, and seasonality of leaf display) influences the global climate through alteration of radiation, momentum, water vapor and heat related fluxes at or near the Earth surface (DeConto et al, 2000). While elevated CO_2 levels in the atmosphere is mostly agreed to be the predominant factor in the warming of the planet, the influence of vegetation feedbacks on Cretaceous warmth is now of interest. Zhou et al. (2012) examined the effect of vegetation on mid-Cretaceous climate simulation by comparing two high atmospheric CO_2 experiment using a fully coupled atmospheric-ocean GCM from the NCAR's community climate system model version 3 (CCSM3) with dynamic vegetation component, where the vegetation component of the coupled model was turned off in one of the simulations. Their studies showed that CO_2 induced warming promotes expansion of high-latitude forests, thereby causing more Polar temperature through lower cloud cover and surface albedo.

The basis of this work is the publication by Klages et al. (2020) where it was suggested that their reconstructed temperate climate at a latitude of ~82 °S requires a combined atmospheric CO_2 forcing of 1,120 – 1,680 ppmvv and a vegetated land surface without

major Antarctic glaciation. In this study, the Cretaceous climate has been simulated using the newly developed AWI- Earth System Model-2 (AWI-ESM-2). The AWI-ESM-2 consists of the FESOM 2.0 with an unstructured mesh CORE2 resolution, the ECHAM6 running on T63 grid, and a land surface scheme (JSBACH) with interactive vegetation dynamics. This work is aimed at enabling the best reasonable representation of the Cretaceous climate forced with different atmospheric CO_2 concentrations using the AWI-ESM-2, including terrestrial vegetation dynamics.

1.4 Thesis structure

While the first chapter introduces the basic motivation, the second chapter describes the AWI-ESM-2 model employed for this study, including its major components and resolutions. Followed by input boundary conditions, experimental design and tools employed in running the model and presenting the results in chapter 3. Chapter 4 describes and discusses the results, which include basic climatic variables like surface temperature, sea-ice, snow depth and precipitation and the vegetation cover types, with a keen interest on the Cretaceous Southern high latitude vegetation cover. Chapter 5 gives a conclusion and an outlook towards possible future investigations.

CHAPTER 2

Methodology

2.1 Model Description

The AWI-ESM-2 (Fig 2.1) was used in this study to simulate the mid-Cretaceous climate. The AWI-ESM-2 is an extension of the AWI Climate Model-2.1 (AWI-CM-2.1) (Sidorenko et al., 2019) with interactive vegetation. This newly developed model includes the atmospheric component ECHAM6, the ocean and sea ice component FESOM 2.0, and the land surface module JSBACH, which resolves the vegetation dynamics to ensure vegetation climate consistency.

AWI-ESM-2 has already been employed successfully in the investigation of the climate of some other time-periods, such as the Holocene (Shi et al., 2020; Brierley et al., 2020), the Last Interglacial (Otto-Bliesner et al., 2020; Kageyama et al., 2020a) and the Last Glacial Maximum (Lohmann et al., 2020; Kageyama et al., 2020b). This study however focuses on the use of AWI-ESM-2 for simulating the mid-Cretaceous climate for the first time, with individual descriptions of each model component given hereafter.

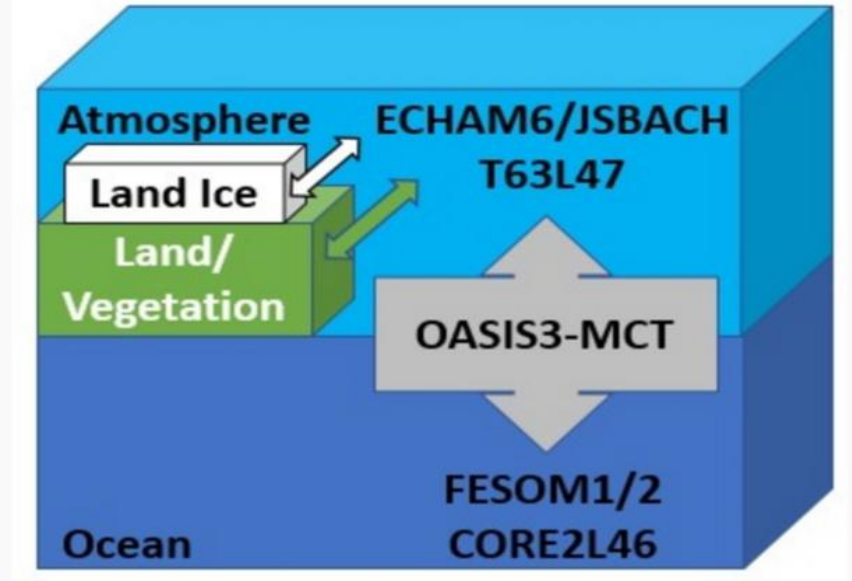

Figure 2.1 Schematic view of the AWI-ESM-2 modeling toolbox

(https://fesom.de/models/awi-esm/)

2.2 The Atmospheric General Circulation Model ECHAM6

The Atmospheric model ECHAM6 is the most recent version of the atmospheric general circulation model, ECHAM; developed as an improvement to ECHAM6 (Roeckner et al, 2003; Roeckner et al, 2006). ECHAM´s development stemmed from an initial version of the global numerical weather prediction model at the European Centre for Medium-Range Weather Forecasts (ECMWF) and has steadily been developed by Max Planck Institute for Meteorology (MPI-M).

ECHAM6 targets the coupling between adiabatic processes and large-scale circulation, which are both driven by radiative forcing (Stevens et al, 2013). It is made up of a dry spectrum-transform dynamical core, a suite of physical parametrizations representing the adiabatic processes, a transport model for scalar quantities and some boundary data sets for externalized parameters, such as trace gas and aerosols dispersal. Significant changes relative to ECHAM5 include: Modification of the radiation schemes to give a better representation of radiative forcing; the surface albedo representation has also been upgraded, including the consideration of melt ponds on sea ice; a highly improved representation of the middle atmosphere as part of the standard model; External data sets describing the

climatological spatial and temporal distribution of aerosol and ozone have been replaced by transient observation-based data sets extended forward to 2100 and backward to 1850 based on the representative concentration pathway scenarios developed for the 15th IPCC Assessment Report (Giorgetta et al, 2013).

ECHAM6 has been configured to operate at five different resolutions.

Version	**Truncation/Levels**	**Description**
CR	T031/L47	Instructional purposes (can also run at L31)
LR	T063/L47	Default resolution (GR15 ocean land mask)
MR	T063/L95	Highly Resolved Middle Atmosphere (TP04 ocean land mask)
HR	T127/L95	Highly Resolution model for exploratory studies
XR	T255/L95	Experimental very high Resolution

(Source: mpimet.mpg.de/en/science/models/mpi-esm/echam)

However, only the CR; LR; and MR model have been successfully coupled to the ocean model for a stable climate production running at atmosphere simulation time steps of 20mins, 10mins, and 10mins respectively.

ECHAM6 is consolidated based on some specified data. The trace gas climatologies are prescribed based on the description by Schmidt et al. (2012). Details of the aerosol climatologies are given by Kinne et al. (2013), stratospheric aerosol is adapted from an extension of the Pinatubo aerosol data set (Stenchikov et al, 1998) and the tropospheric aerosol is described by a fine and coarse mode with 0.5mm radius of separation. For the parametrization of the sub-grid orographic drag and wave generation, a comprehensive information about the sub-grid orography is provided by the Baines & Palmer. (1990). The land surface and vegetation climatologies follows the CMIP5 Atmospheric Model Inter-

comparison Project (AMIP) simulation which was run with land-use transition and prescribed distribution of natural vegetation (Hurtt et al 2011; Remankutty & Foley 1999).

2.3 The Land Vegetation Model JSBACH

JSBACH is the land vegetation component of the Earth System Model, which has been incorporated into the atmosphere model ECHAM6. JSBACH was developed due to desire to investigate coupled climate-carbon dynamics. It involves parameterization of physical facets (heat and water storage as well as atmospheric exchange) and parameterizations depicting the photosynthetic activity of plants, carbon allocation and storage in soils, soil respiration and plants (Girogetta et al, 2013).

JSBACH employs the 1/0, memory handling, parallelization, time stepping and calendar infra-structure of ECHAM (Reick et al, 2021), it also runs on the same grid and time step as ECHAM (Rast et al, 2013). Every JSBACH grid-box is furnished with a base to illustrate the multiformity of land cover types within a grid-box, especially the plant functional types (PFTs). Nonetheless, the JSBACH can still run freely in a stand alone mode with forcing by simulated or observed meteorological data.

Plant functional types (PFTs) are used in JSBACH to represent the diversity of plants based on structural, physiological and phenological characteristics. Thus, every PFT is globally enriched with attributes appropriate to all manner of processes elucidated by the JSBACH model and the specifications can be found in the land cover type library. There are thirteen PFTs developed into JSBACH, describing various trees, crops, shrubs, grasses, and pastures. Eleven of the PFTs (Table 2.1) were used in the model run of this thesis.

Table 2.1: Plant Functional Types (PFTs) employed in the JSBACH simulations.

PFT index	PFT Description
1	Glacier and Tropical Evergreen trees
2	Tropical deciduous trees
3	Extratropical evergreen trees
4	Extratropical deciduous trees
5	Temperate broadleaf evergreen trees
6	Temperature broadleaf deciduous trees
7	Corniferous evergreen trees
8	Corniferous deciduous trees
9	Deciduous shrubs
10	C4 grass
11	Raingreen shrubs

2.4 The Ocean and Sea Ice Model FESOM

The Finite-Element Seaice-Ocean Model (FESOM) is the first full fledged model with a diverse resolution, which is capable of simulating the ocean extensively. Some FESOM based research similar to the influence of local dynamics on the global ocean (Hellmer et al., 2012; Haid & Timmermann, 2013; Wekerle et al., 2013; Haid et al., 2015; Danilov et al., 2017) found the FESOM backed multi-resolution technique to be outstanding and give way to probing the influence of local mechanisms on the ocean at large while employing a moderate computational work (Sein et al, 2018).

The precise FESOM model used in this study is the FESOM 2.0, it is the newest version of FESOM developed on the basis of an earlier version, FESOM 1.4, using its sea ice component, general use interface and code structure (Danilov et al, 2015). The FESOM 2.0 has a new numerical core based on the finite volume method (Danilov et al, 2017). Unlike in FESOM 1.4; where 3D variables are stored as 1D arrays, adding to more fetching time. As well as owner model efficiency, due to separate assessment of the vertices of tetrahedral elements and its derivatives. The FESOM 2.0 has a better numerical efficiency through the use of 2D data storage for a 3D variable, with vertical and horizontal extents. As a result, long cycles are separated into external cycles over nodes or elements and internal cycles over vertical layers. There is also a 2D data of the unstructured mesh that is reused in the internal cycles, thus, FESOM 2.0 presents a clearly defined fluxes and about three-folds speed in comparison to FESOM 1.4, thereby making it the first mature unstructured mesh ocean model with computational efficiency comparable to the state of art structured ocean models (Scholtz et al., 2019). FESOM 2.0 and ECHAM6 are coupled through the OASIS 3 - MCT coupler (Sidorenko et al., 2019).

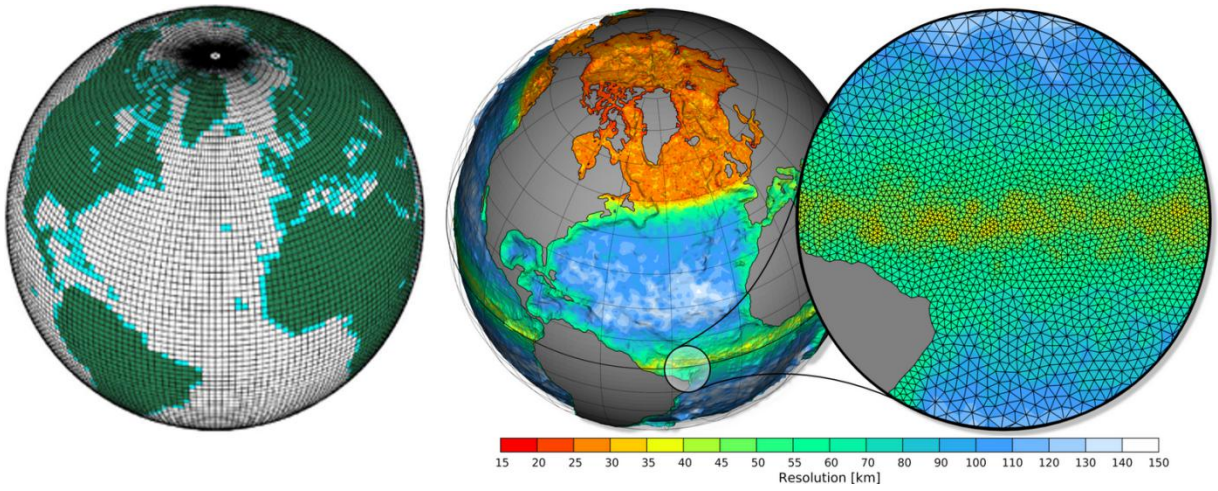

Figure 2.2: ECHAM6 (left) at T63 horizontal resolution and FESOM with 87K grid. FESOM´s colour coding represents the grid resolution in km. Dark area on T63 grid are area where land fraction exceeds 50% while light green area those below 50%. (Figure adapted from Sidorenko et al., 2015).

CHAPTER 3

Data and Methods

3.1 Input Boundary Conditions & FESOM Mesh Resolution

Information about the distribution of sea and the land configuration of a plant during a time period is required in the investigation of the climatic condition on or around the planet at the time of interest. The theory of plate tectonics gives such as basis (William, 2017). However, establishing boundary condition in paleoclimate modelling is often a daunting task, particularly, a period as far back as the Cretaceous. Hence, the continental configuration obtained from plate tectonic modelling as well as Orography and Bathymetry of the Markwick reconstruction is considered in the boundary conditions of this simulations and to produce our land sea mask FESOM mesh after a slight modification, by expanding narrow ocean gateways for unhindered flow. The Cretaceous paleogeography is one of the several available paleogeographies provided by Markwick (2007).

The ocean model FESOM 2.0 uses unstructured grids, putting scaler degrees of freedom at triangle vertices and horizontal velocity on elements. Fig 3.1 shows the land sea distribution with depth levels and elevation of the Cretaceous climate model configuration while Fig 3.2 is the land sea mask and FESOM CORE2 mesh resolution used to simulate the Cretaceous climate. The resolution is increased across the entire Northern and Southern Ocean as well as the equator, so as to produce a good representation of the main oceanographic processes.

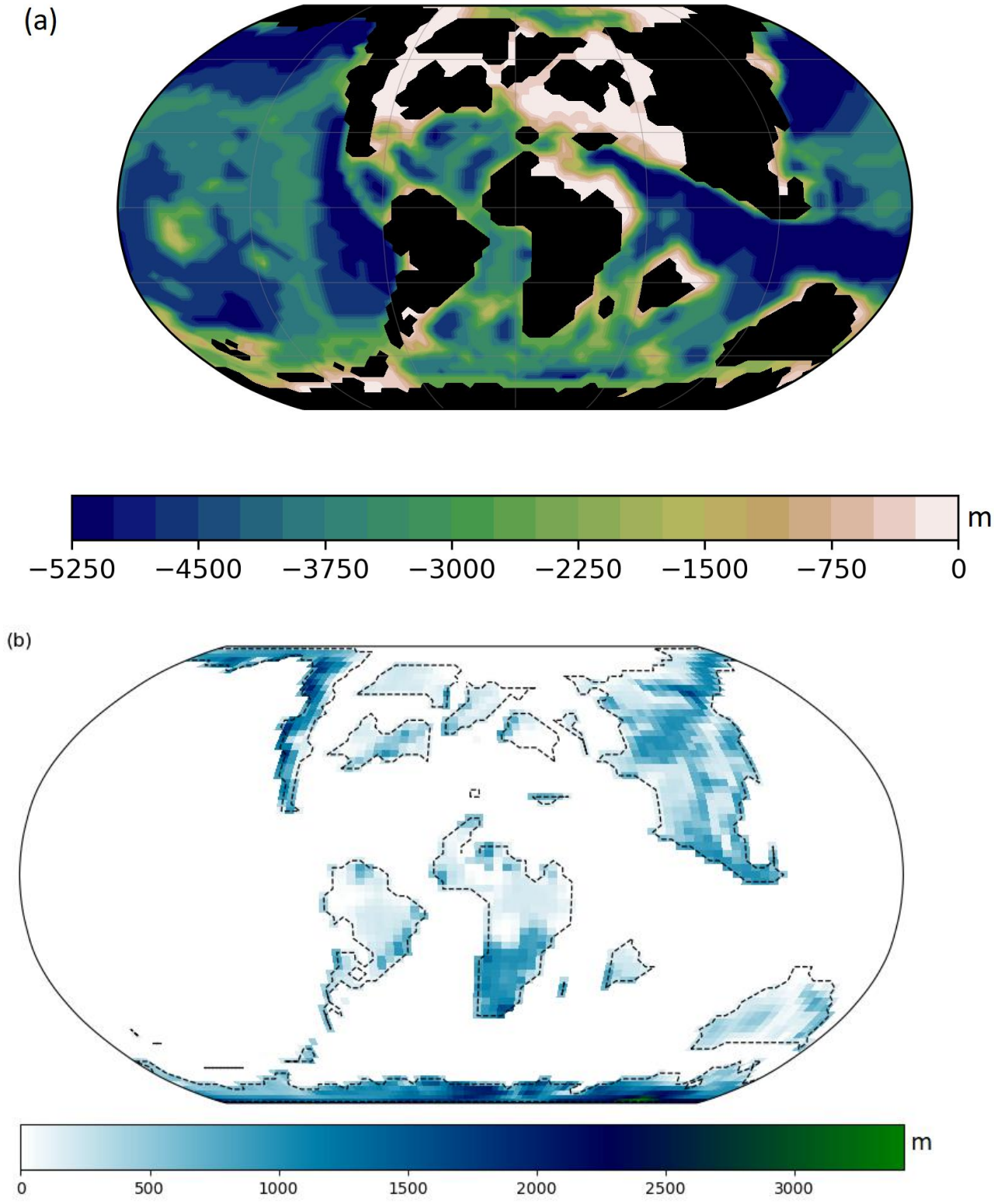

Figure 3.1 Model input boundary conditions used in simulating the mid-Cretaceous (a) Bathymetry and (b) Orography. Units in m.

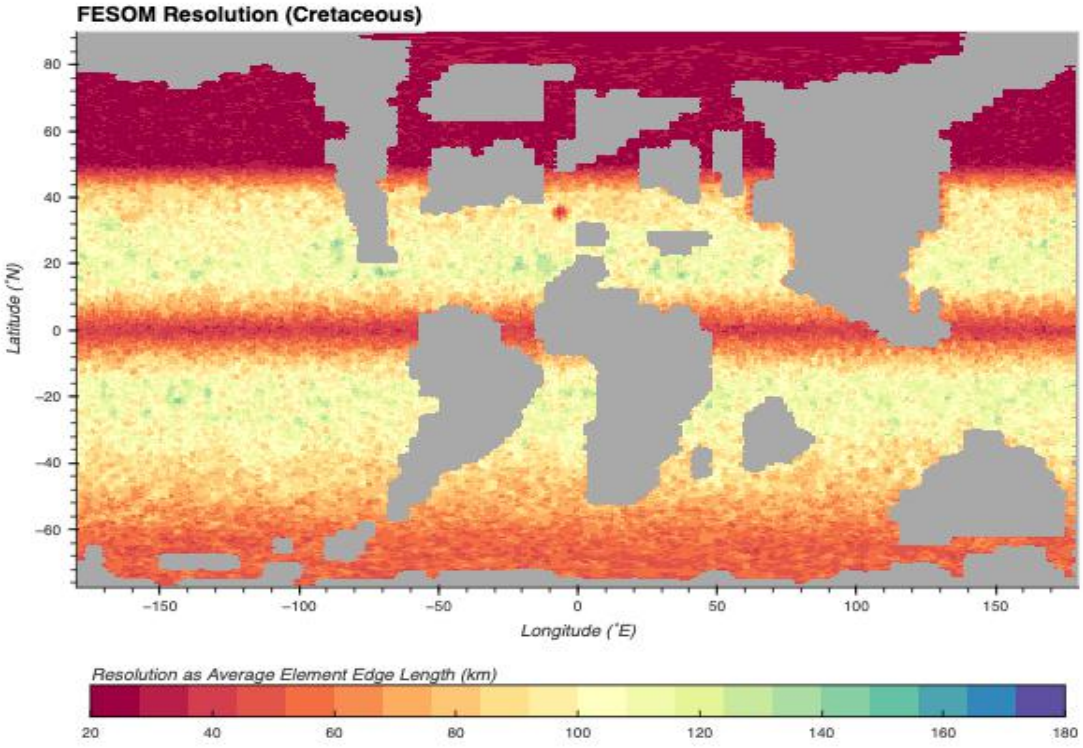

Figure 3.2 Land sea mask FESOM CORE 2 mesh resolution. Units in km.

3.2 Experimental Designs & Forcing

A total of five simulations are involved in this study, three runs were carried out based on Cretaceous simulation using the circulation model AWIESM-2 at low oceanic resolution (the main focus of this work) and two others experiments based on PI climate, which was simulated by other colleagues at AWI Bremerhaven using the AWI-ESM-2. The characteristics of the experiment is given in Table 3.1, where the simulations have been denoted by abbreviations for easier comparison.

Table 3.1 Main Experiment Characteristics

Experimental Acronym	CO2 level (ppmv)	Paleogeography	Integration time
CR_1x	280	90Ma	1000 years
CR_4x	1120	90Ma	1000 years
CR_6x	1680	90Ma	1000 years
PI_1x	280	1850	500 years
PI_4x	1120	1850	600 years

Three simulations were carried out using the Cretaceous palaeogeography as topographic boundary conditions.

Due to uncertainty in the Earth´s orbital dynamics for the pre-Cenozoic times, there are no precise values of orbital parameters (Laskar et al., 2004). Hence, we employed the PI (PI) solar configurations as well as PI solar construct in the model. The Atmospheric concentration of other greenhouse gases (CH_4 and N_20) were also set at PI levels.

To set up the Cretaceous experiments of different Atmospheric CO_2 concentrations highlighted in Table 3.1, an ocean mesh was first produced (Fig. 2b) using the reconstructed Markwick topography Markwick (2007). The ocean model was run in a stand-alone mode for 200years, serving as a base state for the coupled atmosphere-ocean model. The ocean model was simulated with constant salinity and temperature at the beginning of the run, thus starting the model from zero movement in the ocean. Followed by the coupled atmosphere-ocean model, initialized from the ocean only spin up and then integrated for 500 years. The coupled model was subsequently extended for an additional 500 years till an equilibrium state was reached, thus, giving a total integration time of 1000years.

The two other PI simulations were based on PI geography using 280 and 1120ppmvv atmospheric CO_2 values while keeping other atmospheric greenhouse gases (CH_4 and N_2O) constant in both experiments. The PI solar orbital configuration was also employed. Thus, the climate sensitivity is based solely on varying CO_2 concentrations. Results in this study represent climatological average values of the 50 years at the end of every equilibrium integration time.

3.3 Tools used for the Model

CDOs (Climate Data Operators) are a number of command line operators used to analyse and manipulate climate model data. The CDO has been developed to have the same set of processing functions for NetCDF and GRIB datasets in one package and it supports various grid types. It encompasses basic statistical and arithmetic functions, data selection, sub sampling tools, as well as spatial interpolation, making it one of the important tools used for the model.

Ollie is a cluster super computer system at AWI known as Cray CS400. The system has been installed since 2016. It employs the Intel xeon processor E 5- 2600 v4 (Broadwell) and intel's Omni-Path Architecture fabric (hpcwire.com, 2016). Ollie is capable of running advanced climate and environmental research applications, and detailed numerical simulations. Ollie was used in this study to run the AWI-ESM-2 with its sub-models.

Figure 3.3 AWI Cray CS400 Supercomputer

(https://www.awi.de/en/science/special-groups/scientific-computing)

Mistral is the first petascale supercomputer of the Deutsches Klimarechenzentrum GmbH (DKRZ), which is a High Performance Computing system for Earth System research HLRE-3) made up of nearly 3,000 computer nodes, 100,000 computer cores, 240 terabytes storages and 54 petabytes disk size, thus giving it a top execution level of 3.14 PetaFLOPS. Membership of a running HLRE project, official access credentials and acknowledgement of the DKRZ's information processing systems usage guidelines are required to gain access to Mistral (dkrz.de/up/systems/mistral).

Figure 3.4: DKRZ Mistral HLRE3 Supercomputer

(https://www.dkrz.de/de/kommunikation/galerie/Media-DKRZ/hlre-3**)**

3.4 Ocean Salinity and Temperature

The ocean density is the major factor governing the movement of ocean waters; the density is in turn controlled by a mix of temperature and salinity. The simulated ocean temperature and salinity are depicted in Fig 3.1a,b. The temperature decreases polewards while the salinity is high in subtropical and mid-latitude oceans (25^{o} – 40^{o}) between Eurasia and North America, with increased values off the west coast of Africa, east coast of South America, as well as in the central Tethys Ocean.

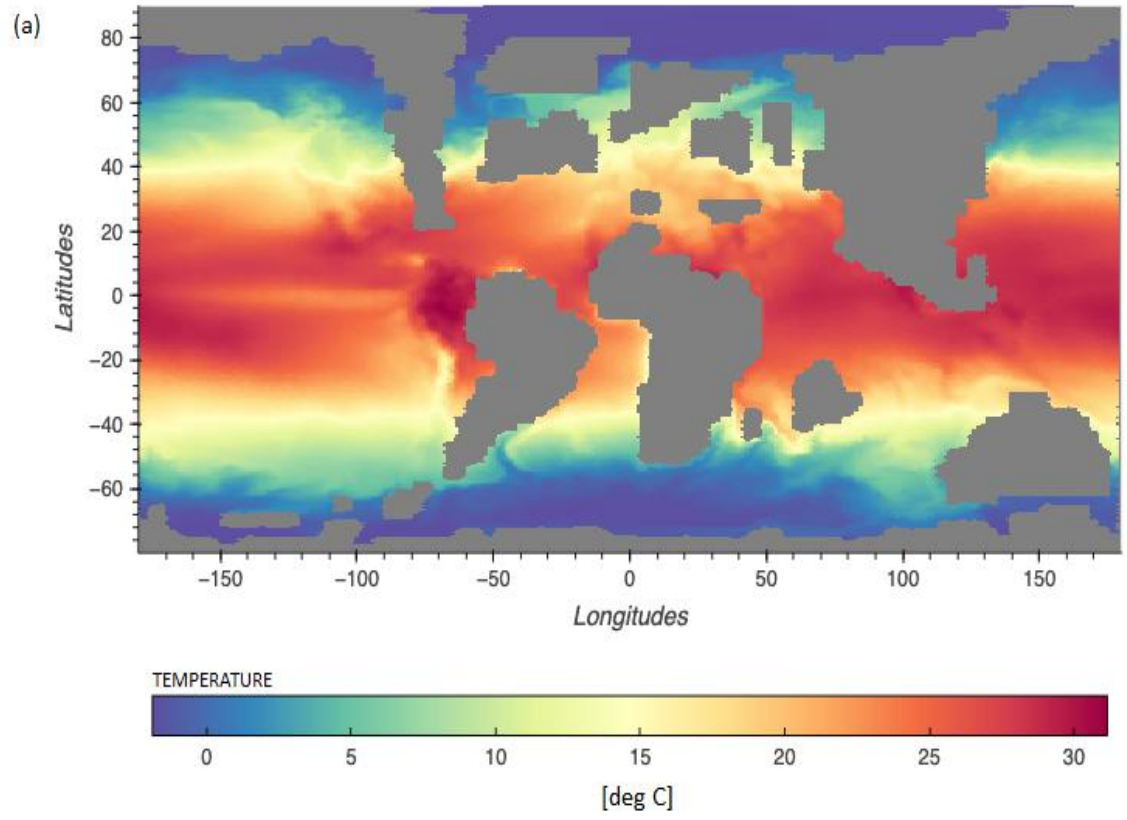

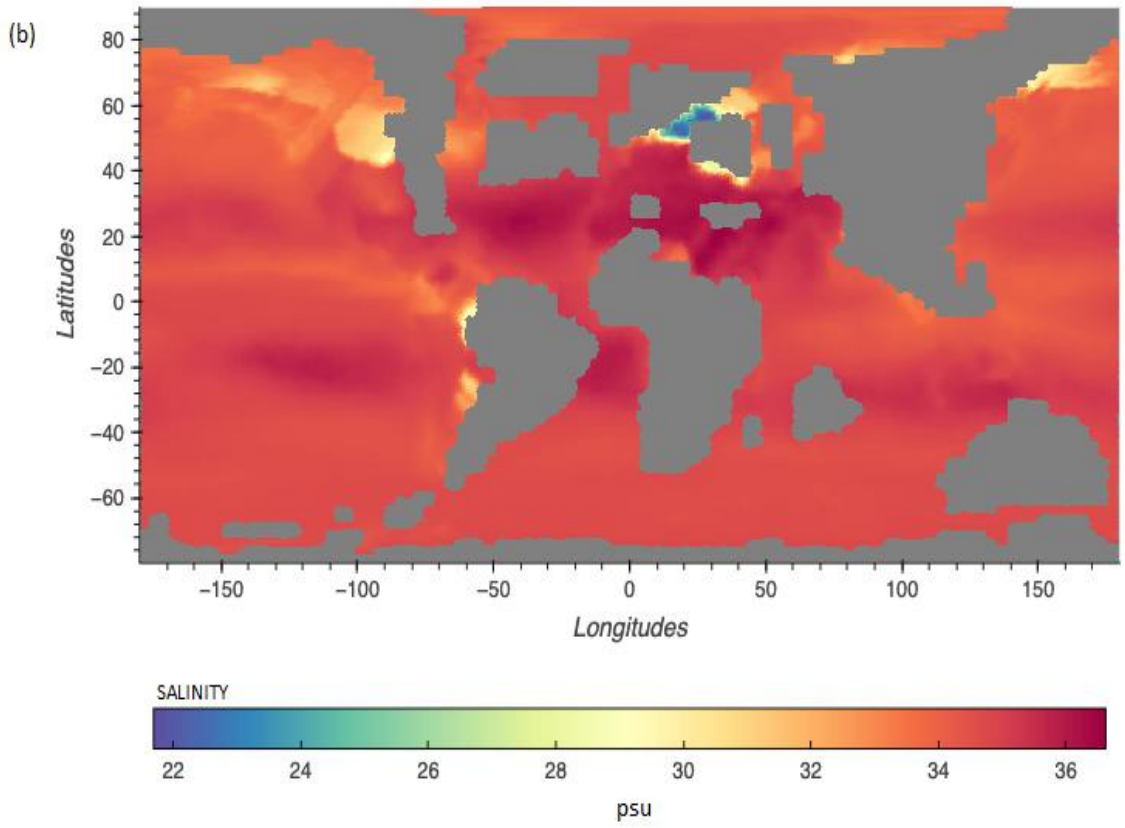

Figure 3.1 The simulated (a) Temperature and (b) Salinity. Units are ^{o}C and PSU respectively.

CHAPTER 4

Results

In this study, the data of five simulations is analyzed. The simulation deviate in terms of prescribed atmospheric CO_2 concentration as well as input boundary conditions. Annual mean and Seasonal climate parameters obtained from all simulations are discussed on a global scale with an additional focus of the Antarctic region.

4.1 Annual and Seasonal Variations of the Cretaceous Climate

4.1.1 Surface Temperature

Figure 4.1 shows the time evolution of surface temperature in the Cretaceous simulation under the three CO_2 levels. The CR_1x experiment with 280ppmvv atmospheric CO_2 level shows a stable trend than the other two right from the start of the simulation. However, all the three simulations stabilized after 600years. At the end of the simulations, the CR_1x simulation gives an average temperature of 15˚C while the CR_4x gives 20˚C, which implies a warming of 5˚C, and at CR_6x an average temperature 22˚C indicating a further ~2˚C increase in warming. Changes in climatic variables of the Cretaceous simulations based on increasing atmospheric CO_2 concentrations forms the basis of most of the analysis in this chapter. Only the last 50years of the simulations where all experiments have attained equilibrium is analyzed.

Figure 4.2 shows the simulated surface temperature for the CR_1x, CR_4x and CR_6x Cretaceous models. For the annual mean as well as for the winter and summer seasons, a higher CO_2 level led to more warming. In the case of annual mean, surface temperature rose from 33°C in CR_1x to 40°C in CR_4x, increasing by 7°C and further increased by ~3° in CR_6x. A vivid increase in surface temperature with increasing CO_2 is seen in the Northern

high latitude during the JJA season, this represents the boreal summer and austral winter. The surface temperature during the JJA season was particularly higher in the central to southern part of the Eurasian continent, with more than 52^{o}C observed in some locations on the CR_6x simulation. In similar manner to the annual mean, the least surface temperature is seen in the CR_1x simulation of the JJA season. Also, during the JJA (Southern Hemisphere winter), there were significant cooling of Antarctica, in the CR_1x simulation, with surface temperature of ~-45°C in parts of Antarctica. Australia gained as much as 15°C in the CR_4x and an additional 9°C in the CR_6x simulation. The Southern Hemisphere winter (DJF) in 4.2 (g- i) exhibits an opposite pattern to the JJA surface temperatures, with south America and Africa being the hottest regions, while the Artic of the CR_1x simulation had very low temperature up to -37°C but warmed up as the CO_2 is increased. Antarctica and Australia had surface temperature of about 23°C in the Southern Hemisphere summer.

In general, tropical surface temperatures were less sensitive to the specified increases in CO_2 than high latitudes.

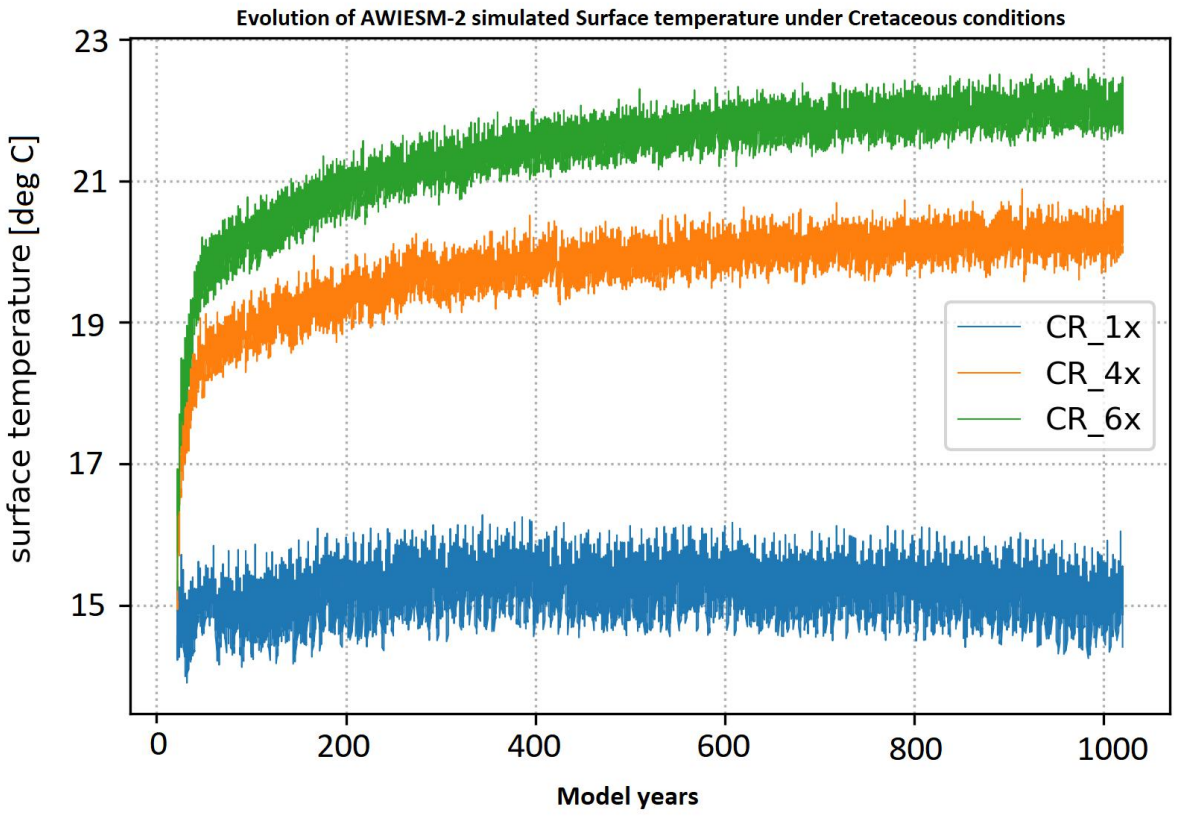

Figure 4.1: Time evolution of the simulated global average surface temperature for the Cretaceous geography. The three experiments are specified by the line colors. Units in Degrees Celcius.

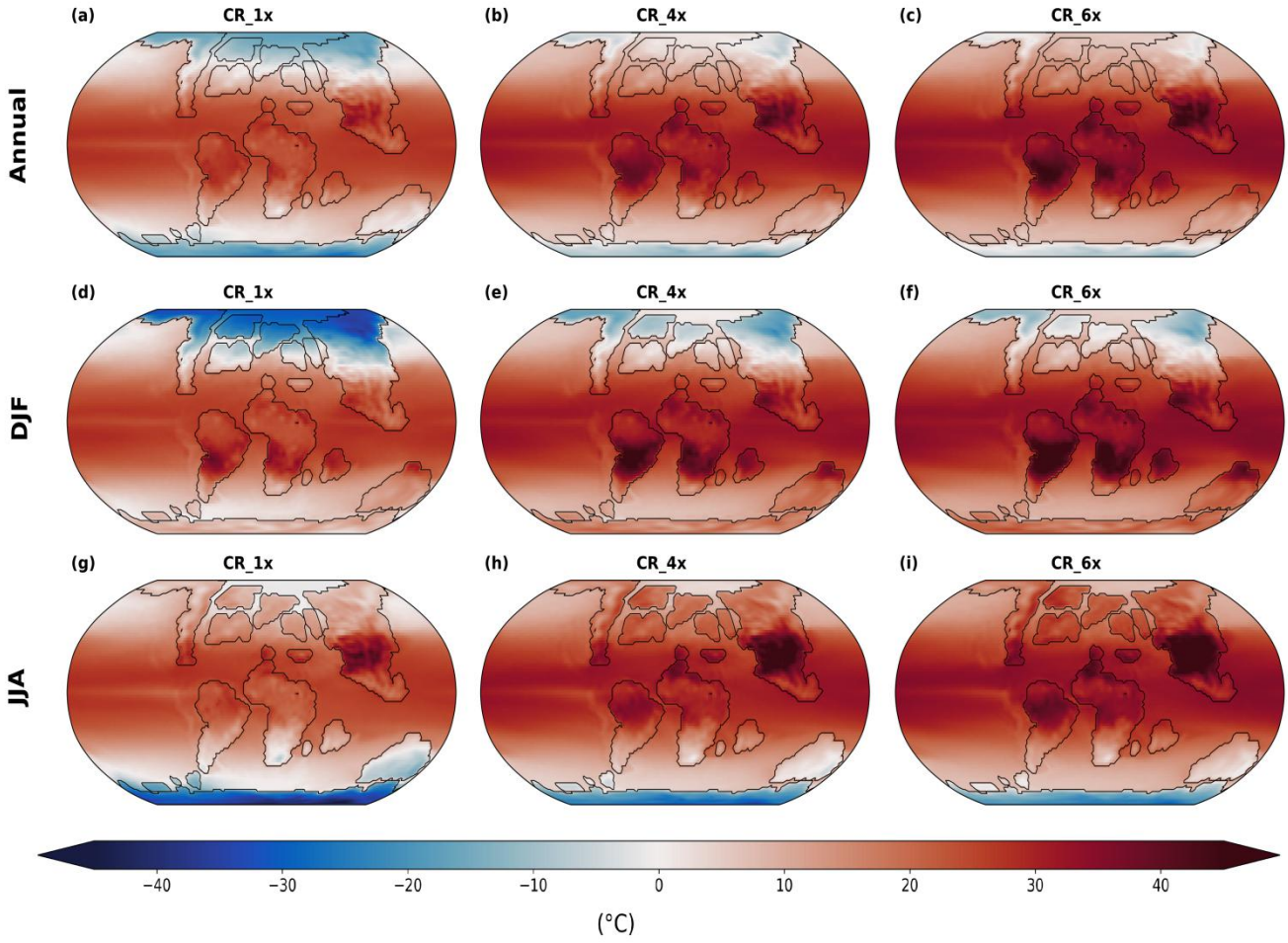

Figure 4.2: Global Surface temperatures of the Cretaceous climate depicted for annual and seasonal mean of experiments CR_1x, CR_4x, CR_6x. (a-c) is the annual mean, (d-f) is the boreal winter, and (g-i) is the boreal summer. Units are °C.

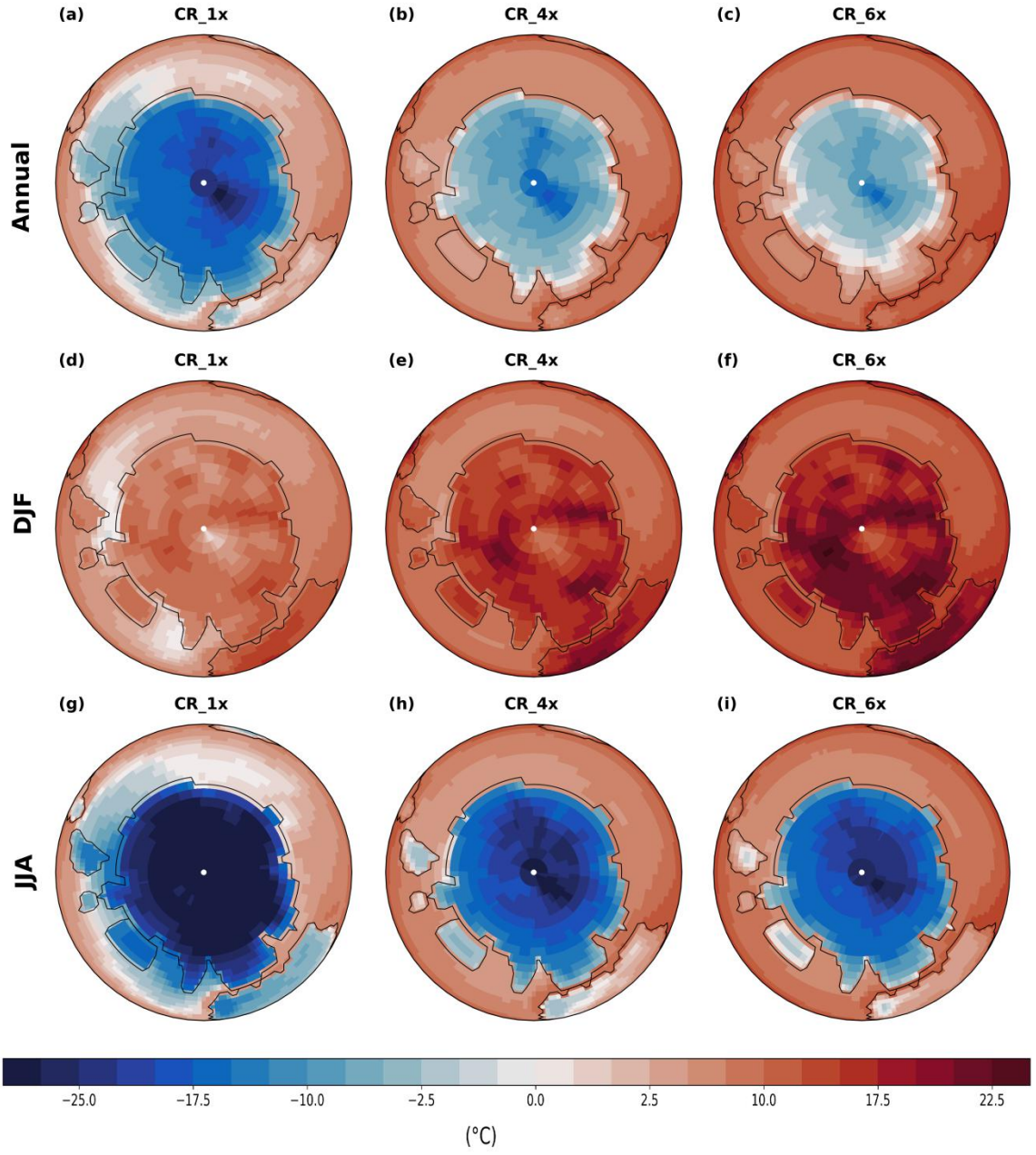

Figure 4.3: Antarctic Surface temperatures of the Cretaceous climate depicted for annual and seasonal mean of experiments CR_1x, CR_4x, CR_6x. (a-c) is the annual mean, (d-f) is the austral summer, and (g-i) is the austral winter. Units are °C.

4.1.2 Snow depth and Sea-ice Cover

The annual mean of snow depth in Fig 4.4(a - c) shows the presence of snow all over Antarctica for CR_4x, CR_4x and CR_6x, as well as in North Eurasia and North America, where a peak snow depth of ~0.27m is exhibited beneath the Asian Alaskan land bridge during the CR_4x simulation. However, a seasonal view reveals the snow depth is only significant in the winter season of the hemisphere being analyzed. In JJA, the Southern Hemisphere winter displays snow presence all over Antarctica in all three simulations, whereas the North America, Eurasia and almost every other continent were completely snow free, with a very low snow presence in South East Australia. An opposite situation is displayed during the DJF, the Southern Hemisphere summer, where the whole of Antarctica and Australia is completely snow free in the high $C0_2$ simulations while the low CO_2 run, CR_1x, exhibits a slight snow presence. North America and North Eurasia displays snow presence with depth close to 0.27m in parts of North America. The simulated Cretaceous sea-ice cover based on 280ppmv, 1,120ppmv and 1680ppmv CO_2 scenario are depicted in Fig 4.6 (a-i). The increase in atmospheric CO_2 concentration of the Cretaceous simulation causes shrinkage of the ice cover in all scenarios considered (annual mean, March, and September). The annual mean shows presence of ice cover in the Arctic and some slight ice also in the west Antarctic waters, the ice cover however reduced in the CR_4x case to the uppermost part of the Arctic and the already low ice cover in West Antarctica is further depleted. At a CR_6x level, ice cover in both the Arctic and Antarctica is almost fully absent. Similarly, no significant ice presence is shown at a CR_6x case in both March and September, inferring that no permanent ice sheet can survive in the high CO_2 mid-Cretaceous climate.

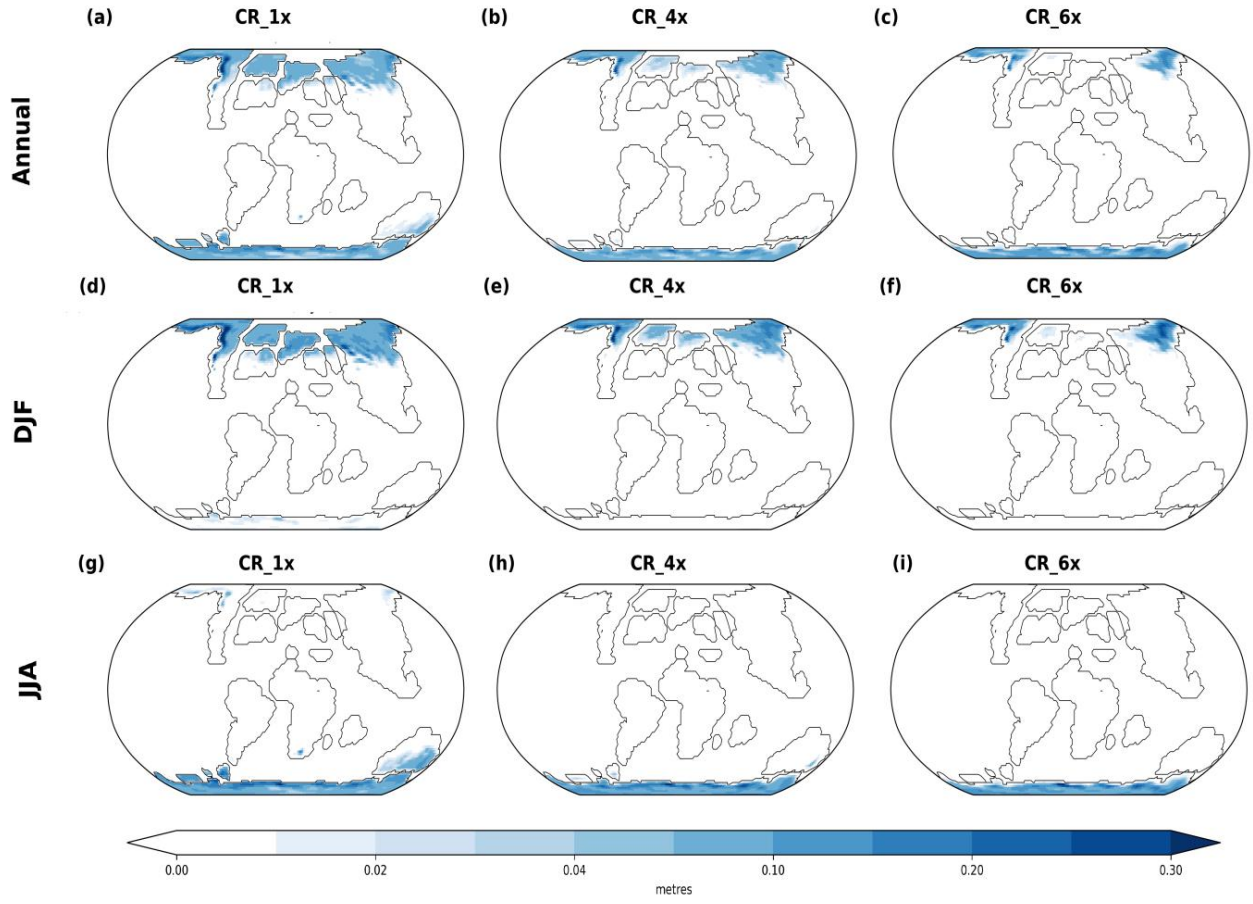

Figure 4.4: Global Snow depth for the Cretaceous climate under CR_1x, CR_4x and CR_6x experiments for annual mean (a - c) and seasonal mean: DJF(d - f) and JJA (g - i). Units are m.

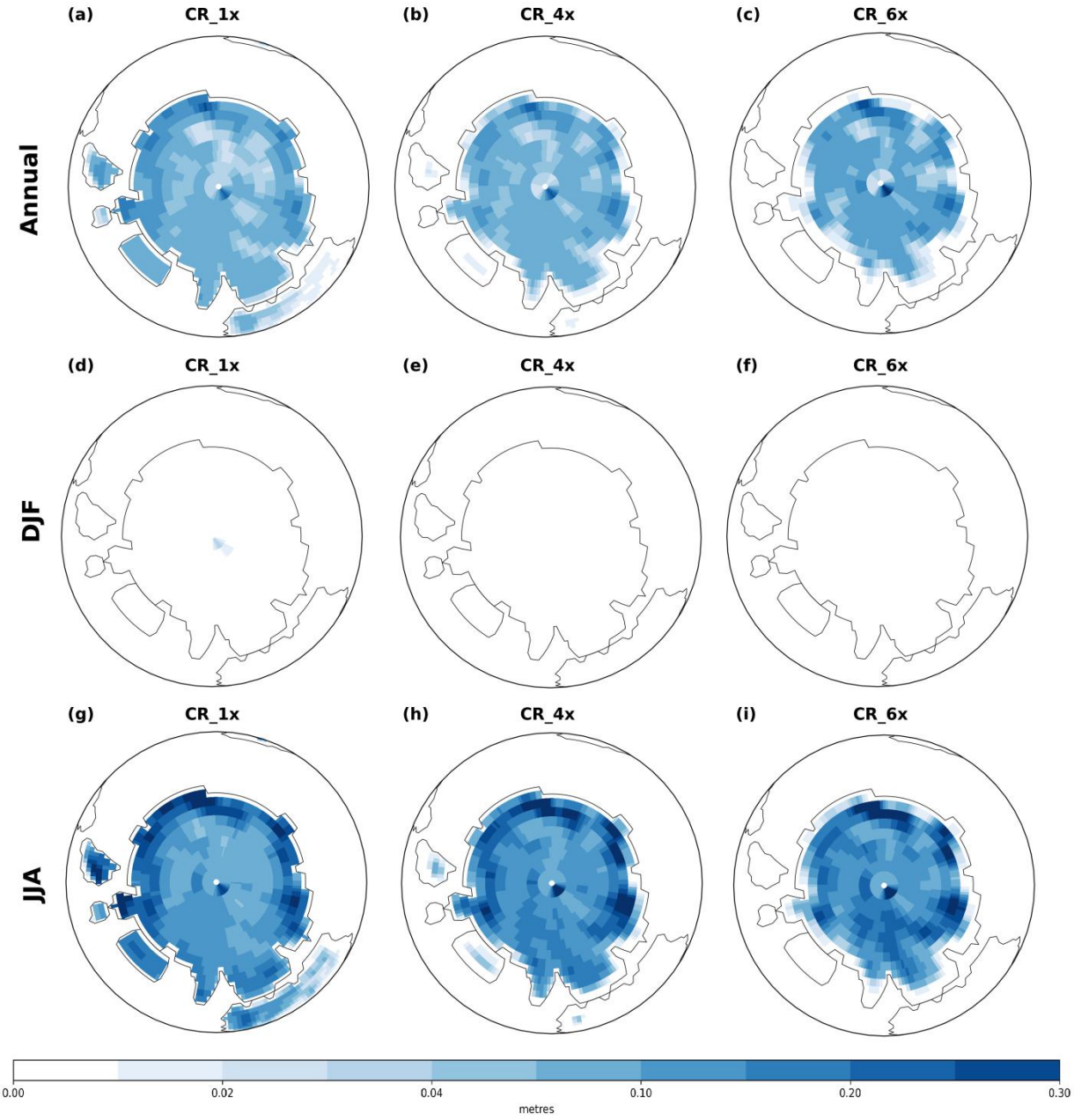

Figure 4.5: Antarctic Snow depth for the Cretaceous climate under CR_1x, CR_4x and CR_6x experiments for annual mean (a - c) and seasonal mean: DJF(d - f) and JJA (g - i). Units are m.

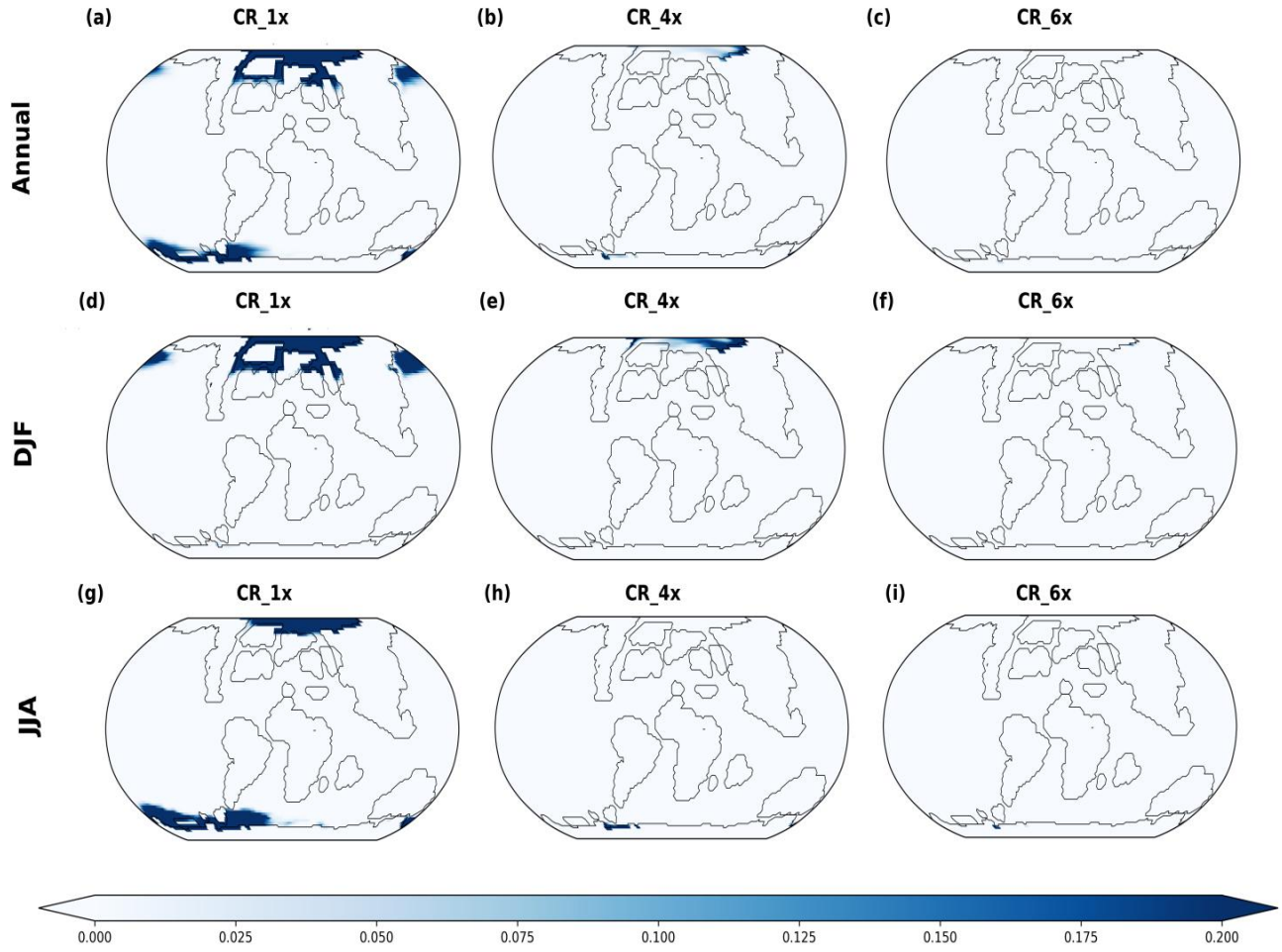

Figure 4.6: Global Sea ice cover under CR_1x, CR_4x and CR_6x experiments for annual mean (a - c) and seasonal mean: DJF(d - f) and JJA (g - i).

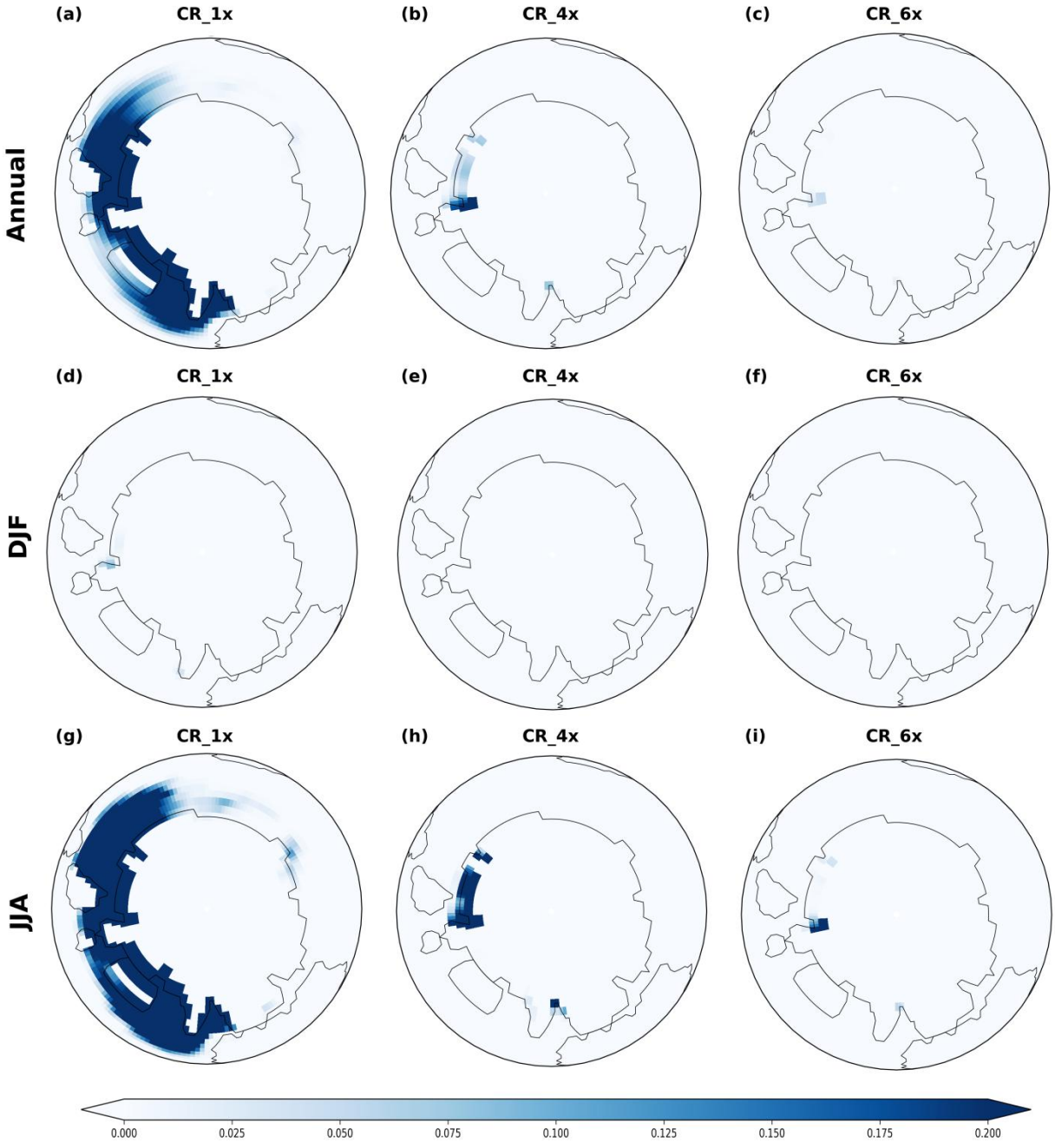

Figure 4.7: Antarctic Sea ice cover under CR_1x, CR_4x and CR_6x experiments for annual mean (a - c) and seasonal mean: DJF(d - f) and JJA (g - i).

4.1.3 Precipitation

The precipitation for the mid-Cretaceous climate simulated for the CR_4xand CR_6x scenario is subtracted from the CR_1x and presented in Figure 4.8. Overall, the effect of CO_2 increase on the mid-Cretaceous simulations is not easily foreseeable for the precipitation as in the case of surface temperatures. The annual precipitation increased in the tropics in the CR_6x - 1x scenario. There was also a slight increase in the high-latitude precipitation, specifically the North Pacific. The JJA season is significantly wetter with more precipitation in the CR_6x - 1x scenario than the CR_4x -1x. The tropics are wetter than all other regions, and the Southern high latitudes are not really affected by the increased CO_2 in both seasons.

The higher precipitation of the CR_6x - 1x around the tropics to South-east Asia and the North Pacific suggests a probable monsoon with a higher CO_2 level in the Northern Hemisphere summer.

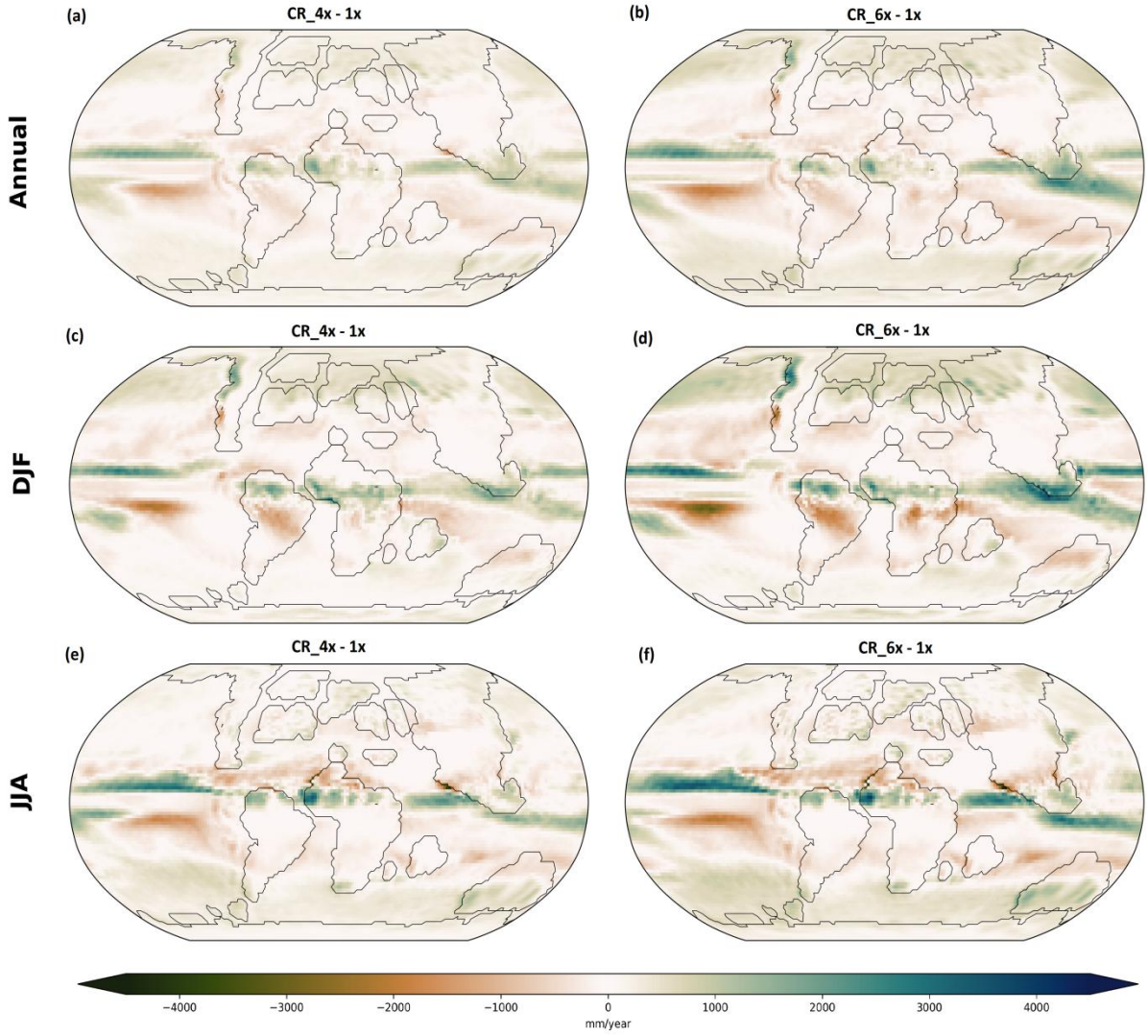

Figure 4.8 Simulated precipitation anomalies of the Cretaceous climate depicted for CR_4x and CR_6x relative to CR_1x for annual mean (a, b) and seasonal mean: DJF(c, d) and JJA (e, f). Units are mm/year.

4.2 Comparison between AWI-ESM-2 simulations for PI and Cretaceous Climate

4.2.1 Surface Temperature

The Cretaceous simulation employs sea ice configuration, land-sea mask as well as orography which strongly different differs from the PI simulation. Based on the simulation results presented for both periods with prescribed CO_2 concentration of 280ppmvv in Fig 4.9 and 1,120ppmvv in Fig 4.10. The mid-Cretaceous climate proves to be warmer than the PI climate, even at same levels of atmospheric CO_2.

The continents in both simulations generally exhibits huge temperature differences than the oceans due to lower heat capacity of oceans as compared to lands, leading to rapid continental warm up. The most pronounced increased warming is in the austral summer of the Cretaceous. Thus, a polar stereo-graphic view focusing on the South pole region follows in Fig 4.11 and 4.12 for atmospheric CO_2 of 280ppmv and 1120ppmv respectively.

For the 280ppmv CO_2 concentration comparison of PI and mid-Cretaceous experiment is given in figure 4.9, the Antarctic continent exhibited a seasonal dependent warming/cooling in the CR_1x experiment unlike the PI_1x where, although, there was a little warming in Antarctica, it still remained cool, with temperature as less than - 35 ^{0} C. In the Northern hemisphere, there exist some spatial heterogeneity in the PI control experiment particularly in Greenland, Boreal summer temperature was cooler in Greenland compared to other land areas in the Northern Hemisphere as well as distinct cooling above India. The intense summer warming is displayed in Sahel to Sahara and middle eastern region of the PI climate while the Cretaceous exhibited similar warming in Central to Southern Eurasia.

A comparison of PI and mid-Cretaceous run with CO_2 concentration of 1,120ppmv exhibits similar pattern to the CR_1x and PI_1x simulations, with a general increase in warming in both simulations with surface temperature gains as high as 7°C in some regions.

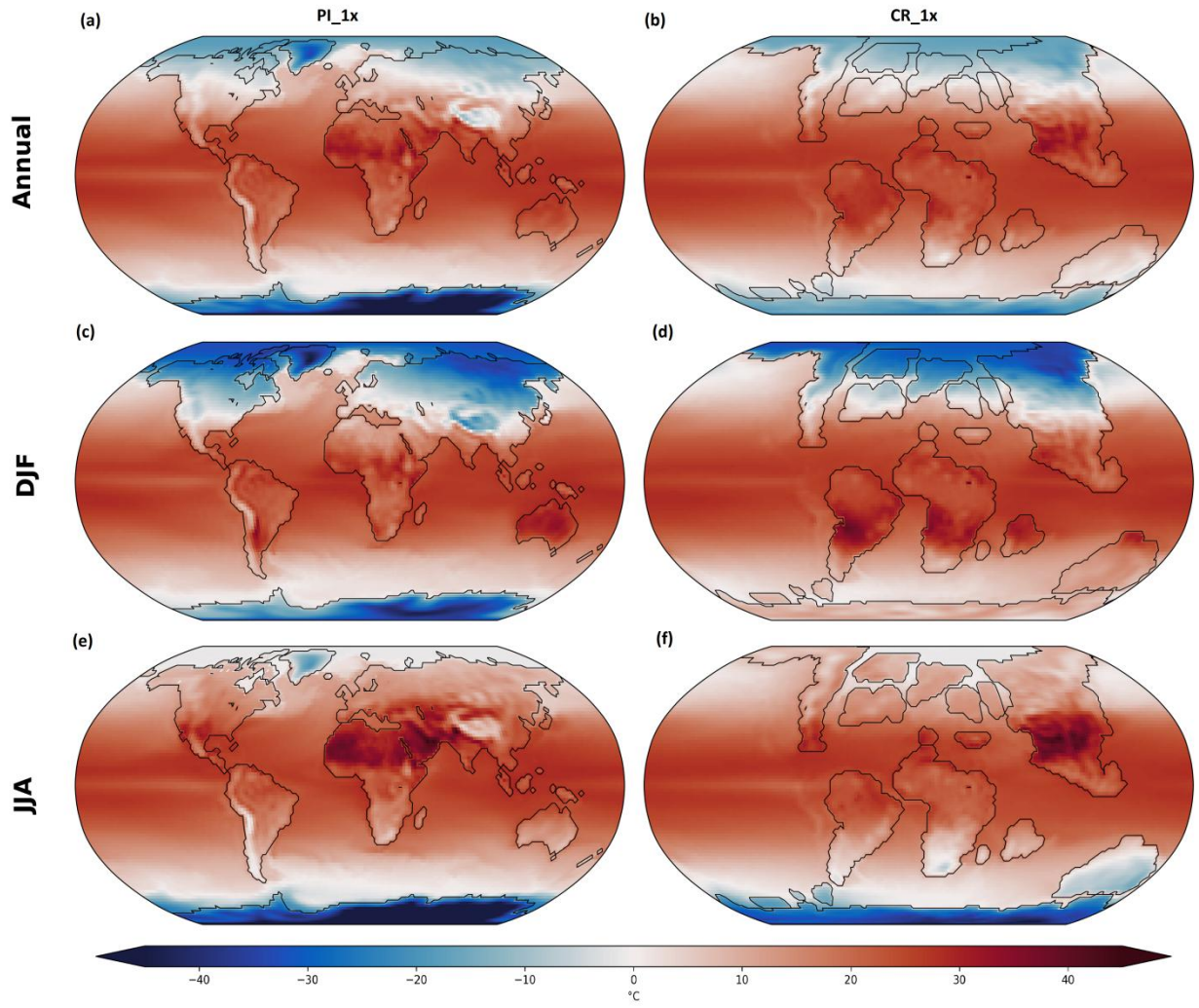

Figure 4.9: Comparison between Surface temperature of the PI and mid-Cretaceous Climate depicted for annual and seasonal mean of PI_1x and CR_1x. (a, b) is the annual mean (c,d) is the winter and (e, f) is summer. Units are ^{o}C.

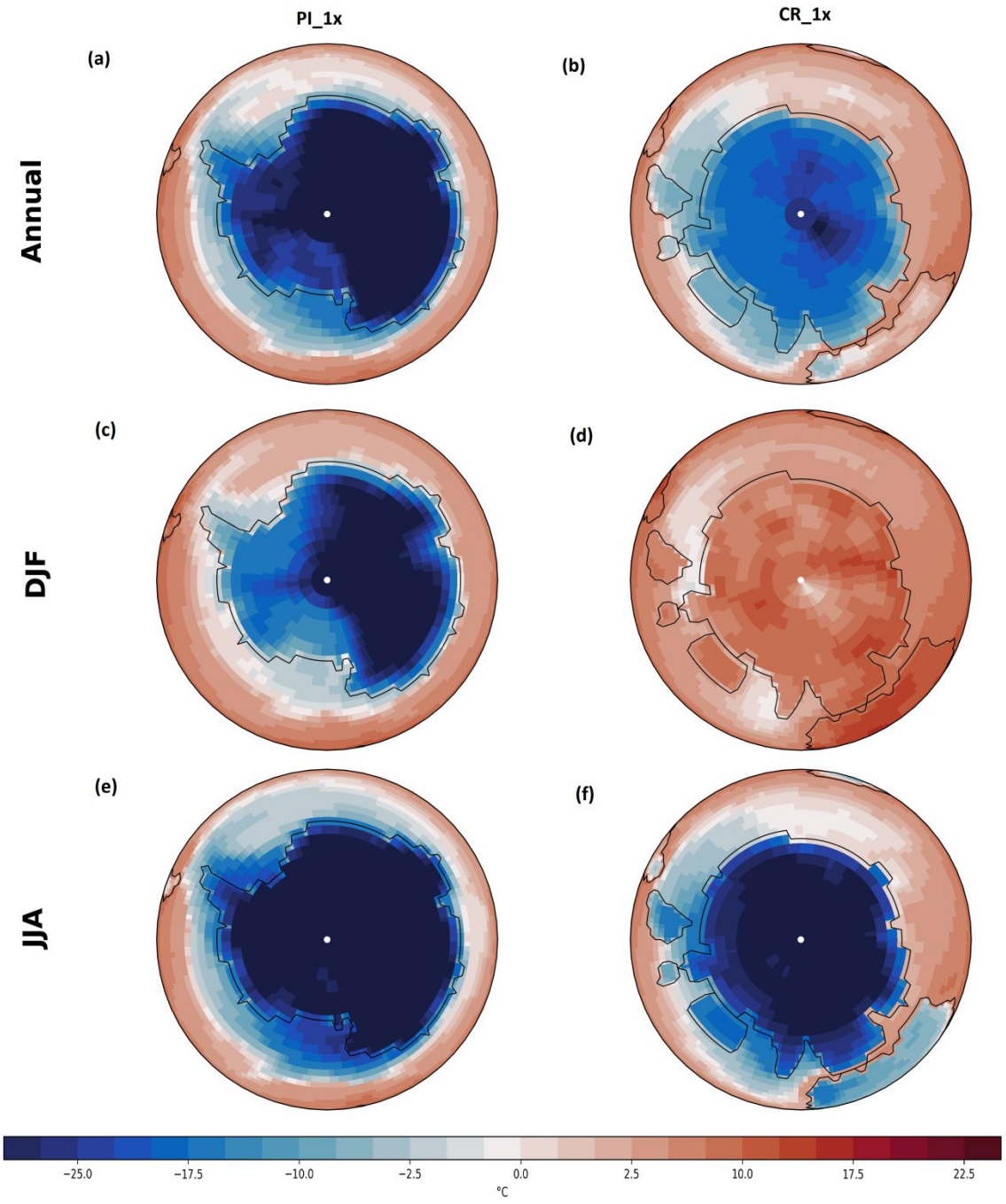

Figure 4.10: Comparison between Antarctic Surface temperature of the PI and mid-Cretaceous Climate depicted for annual and seasonal mean of PI_1x and CR_1x. (a, b) is the annual mean (c,d) is the winter and (e, f) is summer. Units are ^{o}C.

.

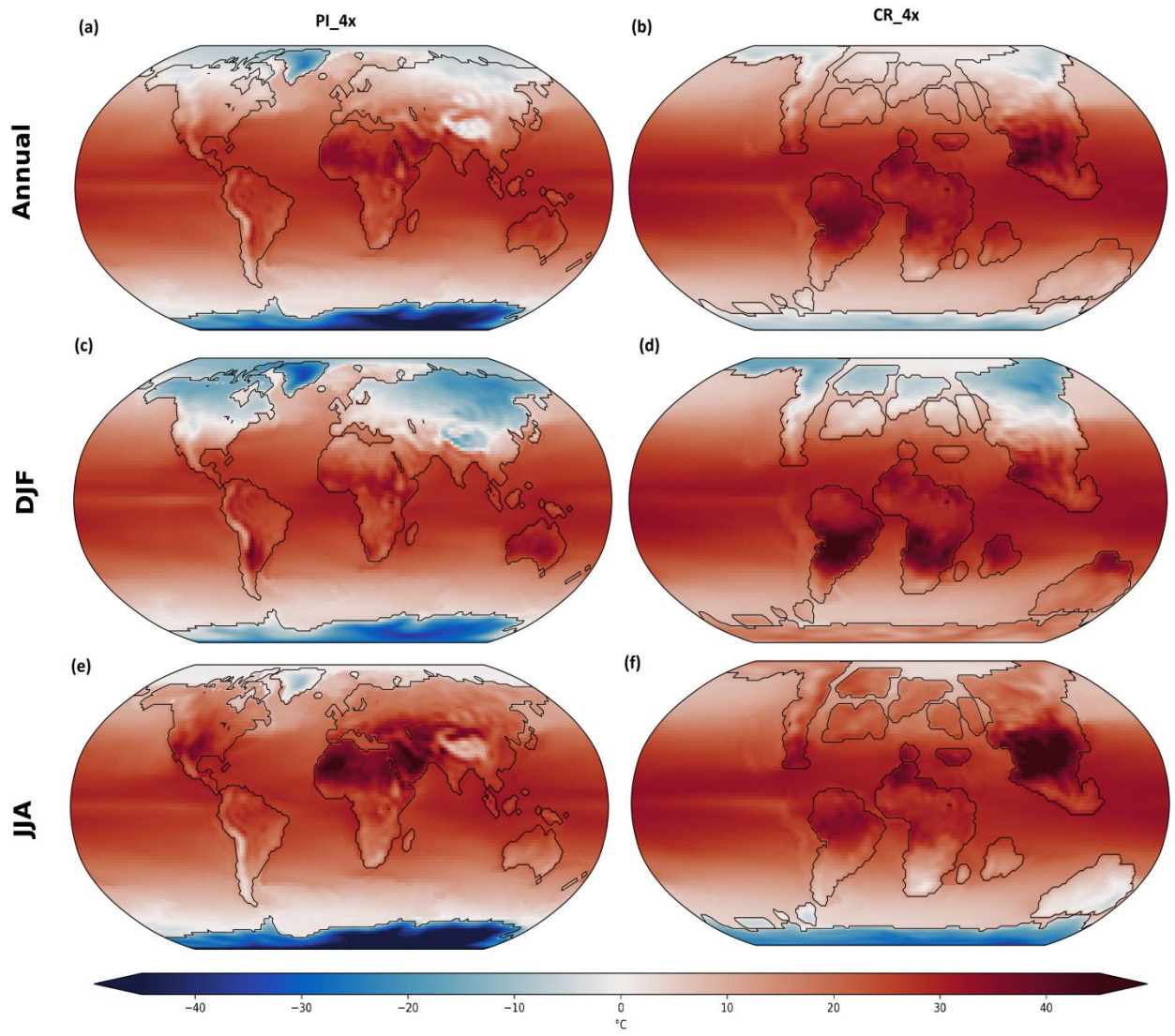

Figure 4.11: Comparison between Surface temperature of the PI and mid-Cretaceous Climate depicted for annual and seasonal mean of PI_4x and CR_4x. (a, b) is the annual mean (c,d) is the winter and (e, f) is summer. Units are ^{o}C.

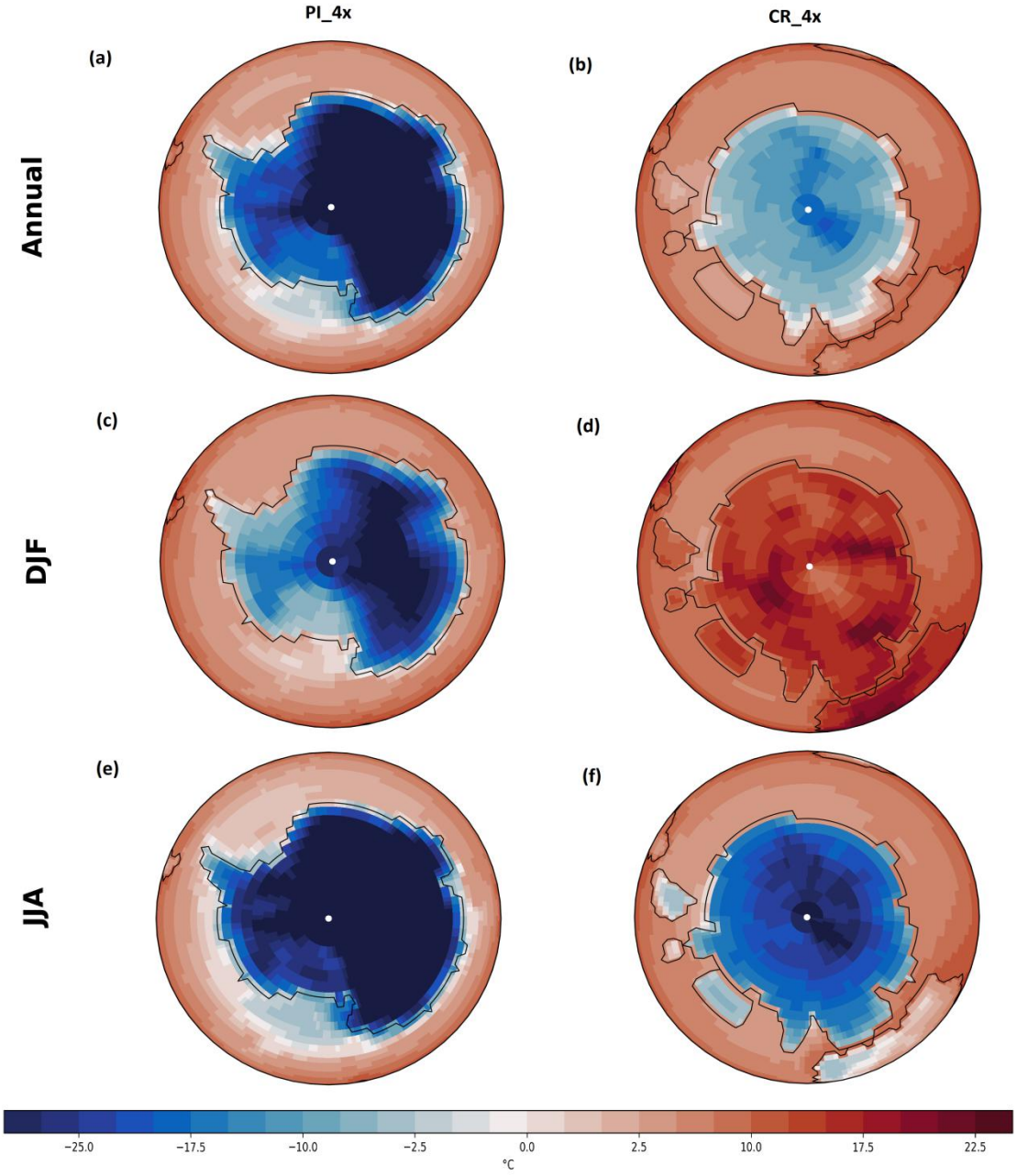

Figure 4.12: Comparison between Antarctic Surface temperature of the PI and mid-Cretaceous Climate depicted for annual and seasonal mean of PI_4x and CR_4x. (a, b) is the annual mean (c,d) is the winter and (e, f) is summer. Units are ^{o}C.

4.2.2 Snow depth and Sea-ice cover

Spatial maps of the annual and seasonal snow depth mean of the PI and mid-Cretaceous climate under a CO_2 forcing of 280ppmv are shown in figures 4.13 and 4.14. Both time periods agree that in the DJF season, there's thicker snow on the land areas close to and in the Arctic (from ~ 55^0 upward) with the exception of Greenland in the PI_1x (DJF) simulation where the snow deposit is only present in a few areas, South of Greenland with other parts of Greenland being snow free and the Himalayas had snow deposit of about 23cm thick, while the Southern Hemisphere during the DJF season had just a slight snow presence in CR_1x. Closer examination of the Antarctic on Fig 4.14 shows a build-up of about 2cm thick snow in the center of Antarctica during the CR_1x simulation only.

In contrast to the Boreal winter, the summer season has very small snow accumulation in the Arctic, approximately 3cm of snow is present in North east Eurasia and North America during the Cretaceous, same level is also observed in Siberia and Northern Canada during the PI_1x. However, in the JJA, Southern Hemisphere of the PI_1x is without snow accumulation but the CR_1x in JJA exhibits snow accumulation all over Antarctica with about 30cm in some parts and there is an extension of the snow deposit to Southern parts of Australia and South Africa. The Australian and African continent during the Cretaceous period were closer to Antarctica than the PI.

The comparison maps of the PI and mid-Cretaceous experiment under forcing of 1120 ppmv of atmospheric CO_2 in Fig 4.15 and 4.16 follows a similar pattern to the CR_1x and PI_1x experiments, with thick snow in the Arctic during the DJF season. However, the snow coverage is reduced as the CO_2 level in the atmosphere is quadrupled. The Antarctic view in Fig 4.22 also shows that for DJF, both PI_4x and CR_4x are free of snow accumulation.

For the Sea-ice cover, plots of the mean annual, winter and summer sea-ice concentration during the simulated PI and mid-Cretaceous climate with CO_2 concentration of 280 ppmv are shown in Fig 4.17. It reveals the presence of Sea-ice in the Arctic at all times of the PI climate including the northern part of the Caspian sea during the winter season, there is also large ice concentration in the Cretaceous winter, however, it diminishes in summer, reducing to only the Arctic ocean. However, Sea-ice in the Austral winter is more

concentrated in western Antarctica than the east. The 1,120 ppmv atmospheric CO_2 concentration employed in the PI and mid-Cretaceous simulation is presented in Fig 4.19. Unlike the PI_1x case where Sea-ice was present at everywhere in the Arctic, here, it is completely absent in the summer season of both hemisphere while the concentration during the winter season is reduced. Although a significant amount of ice was still present in the PI Arctic, the mid-Cretaceous sea-ice was only concentrated in the shores of North Eurasia. In Austral winter, sea-ice were concentrated all over the shores of Antarctica in PI_4x but in reduced concentration while the CR_4x had very small amount of sea-ice in western Antarctica.

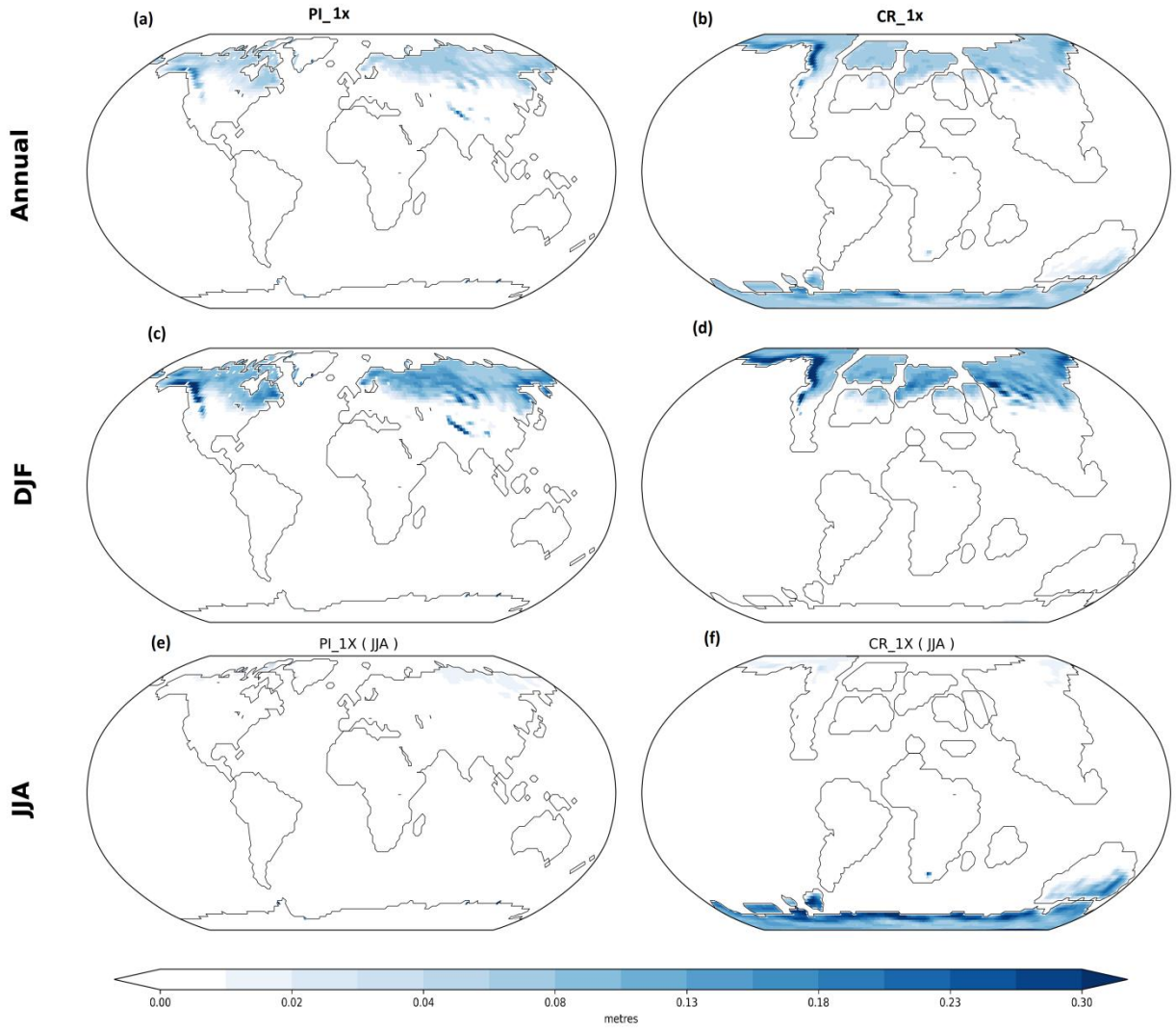

Figure 4.13: Comparison between Snow depth of the PI and mid-Cretaceous Climate depicted for annual and seasonal mean of PI_1x and CR_1x. (a, b) is the annual mean (c,d) is the winter and (e, f) is summer. Units are meters.

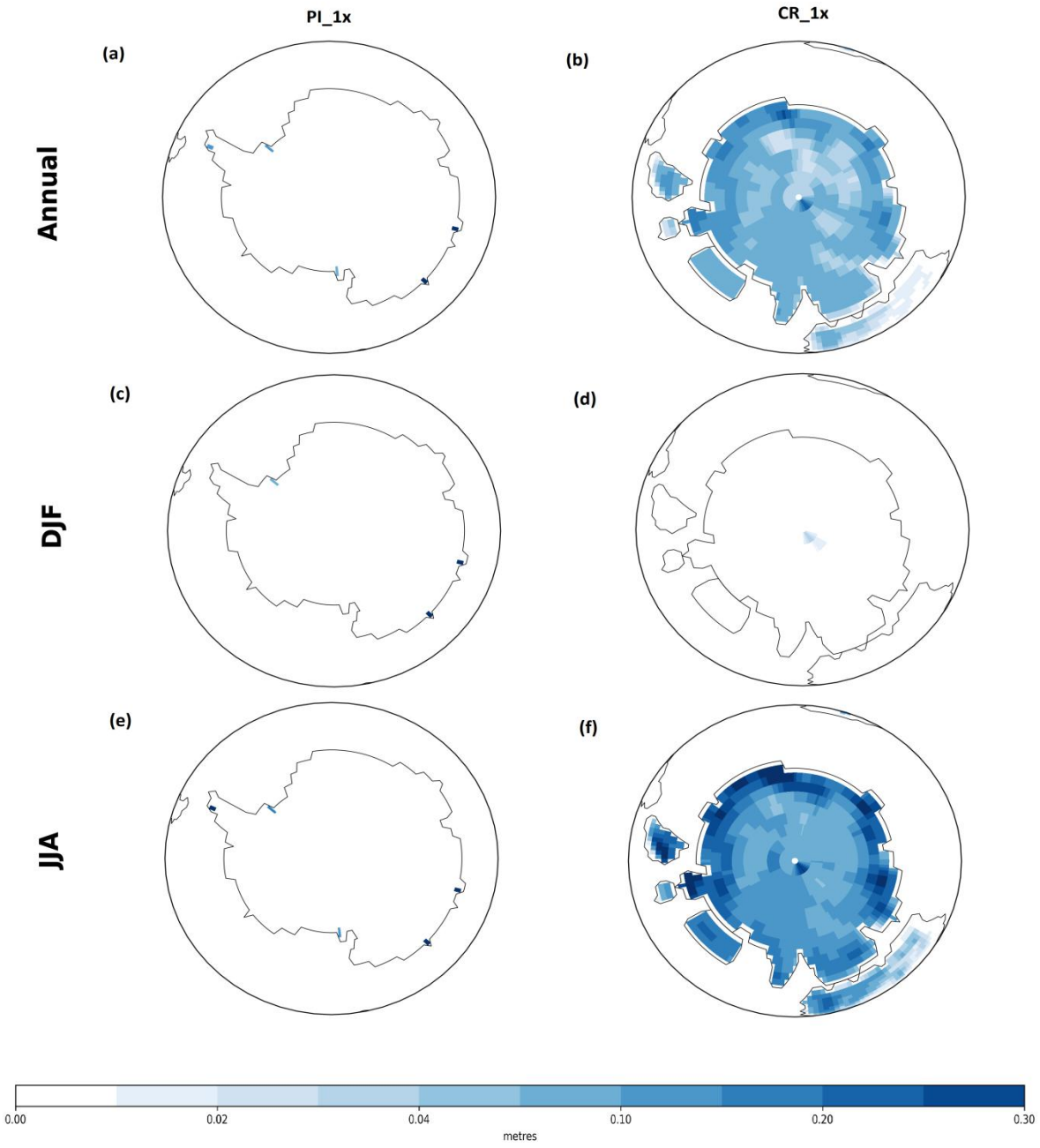

Figure 4.14: Comparison between Antarctic Snow depth of the PI and mid-Cretaceous Climate depicted for annual and seasonal mean of PI_1x and CR_1x. (a, b) is the annual mean (c,d) is the winter and (e, f) is summer. Units are meters.

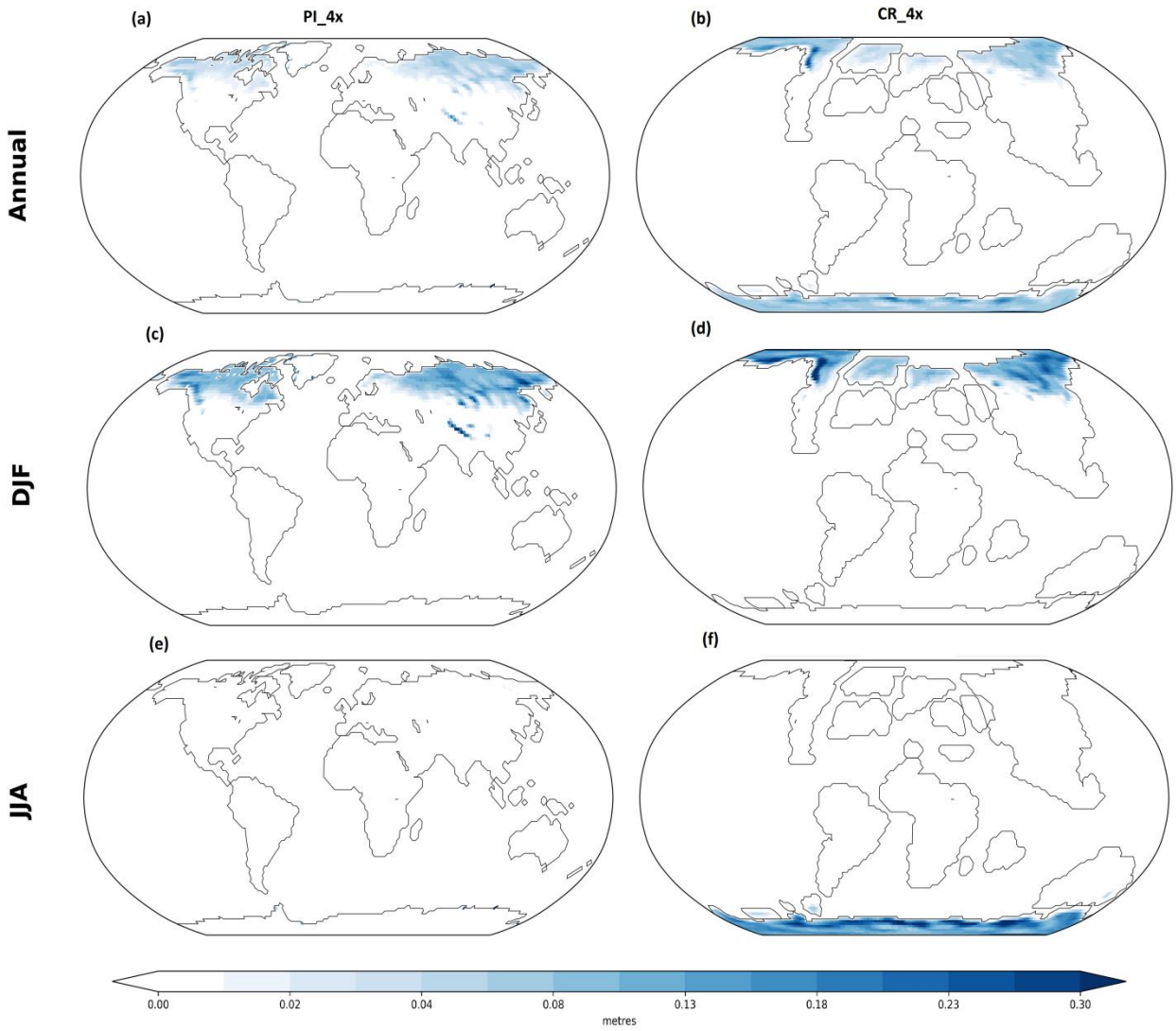

Figure 4.15: Comparison between Snow depth of the PI and mid-Cretaceous Climate depicted for annual and seasonal mean of PI_4x and CR_4x. (a, b) is the annual mean (c,d) is the winter and (e, f) is summer. Units are meters.

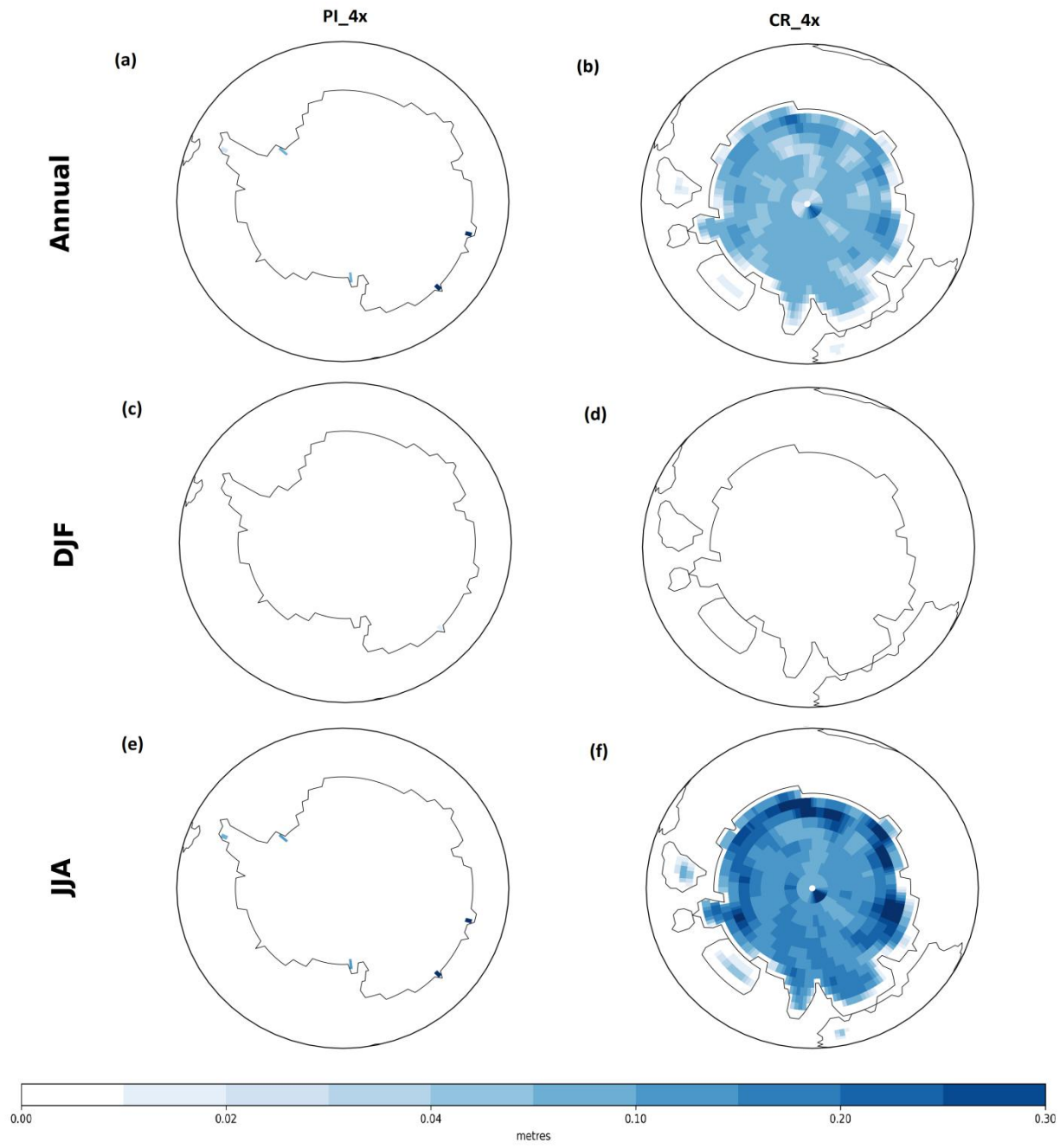

Figure 4.16: Comparison between Antarctic Snow depth of the PI and mid-Cretaceous Climate depicted for annual and seasonal mean of PI_4x and CR_4x. (a, b) is the annual mean (c,d) is the winter and (e, f) is summer. Units are meters.

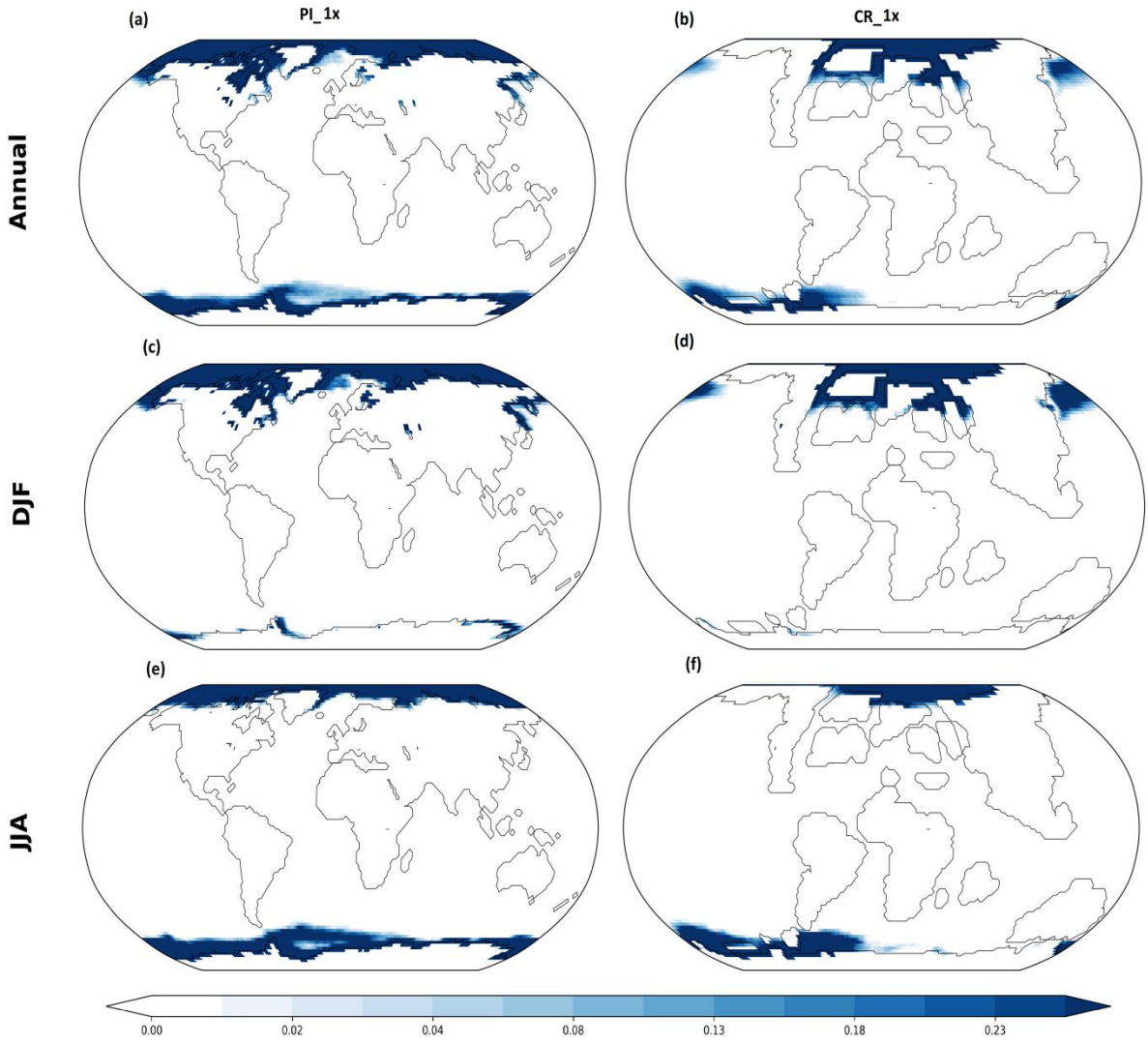

Figure 4.17: Comparison between seaice of the PI and mid-Cretaceous Climate depicted for annual and seasonal mean of PI_1x and CR_1x. (a, b) is the annual mean (c,d) is the winter and (e, f) is summer.

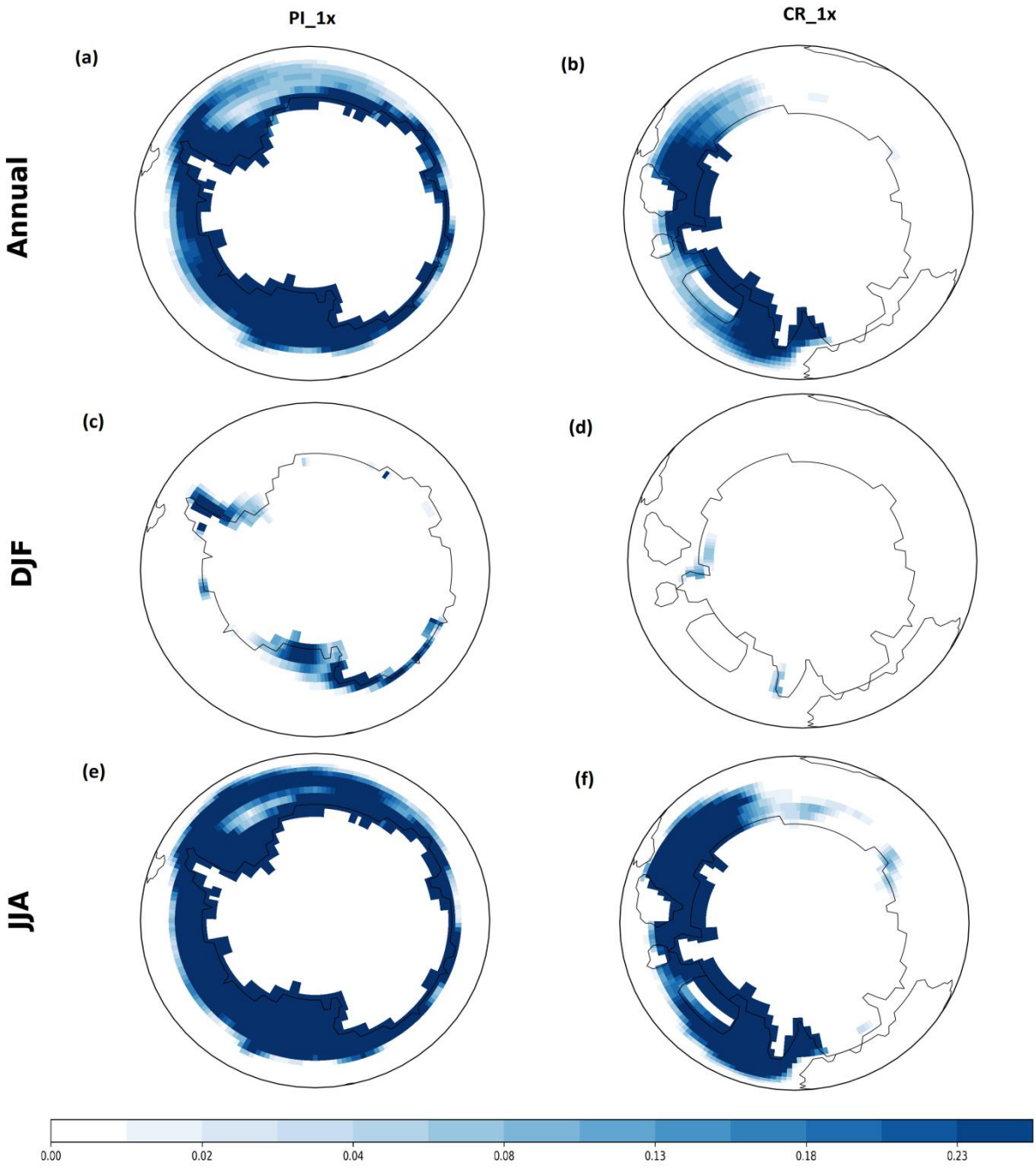

Figure 4.18: Comparison between Antarctic seaice of the PI and mid-Cretaceous Climate depicted for annual and seasonal mean of PI_1x and CR_1x. (a, b) is the annual mean (c,d) is the winter and (e, f) is summer.

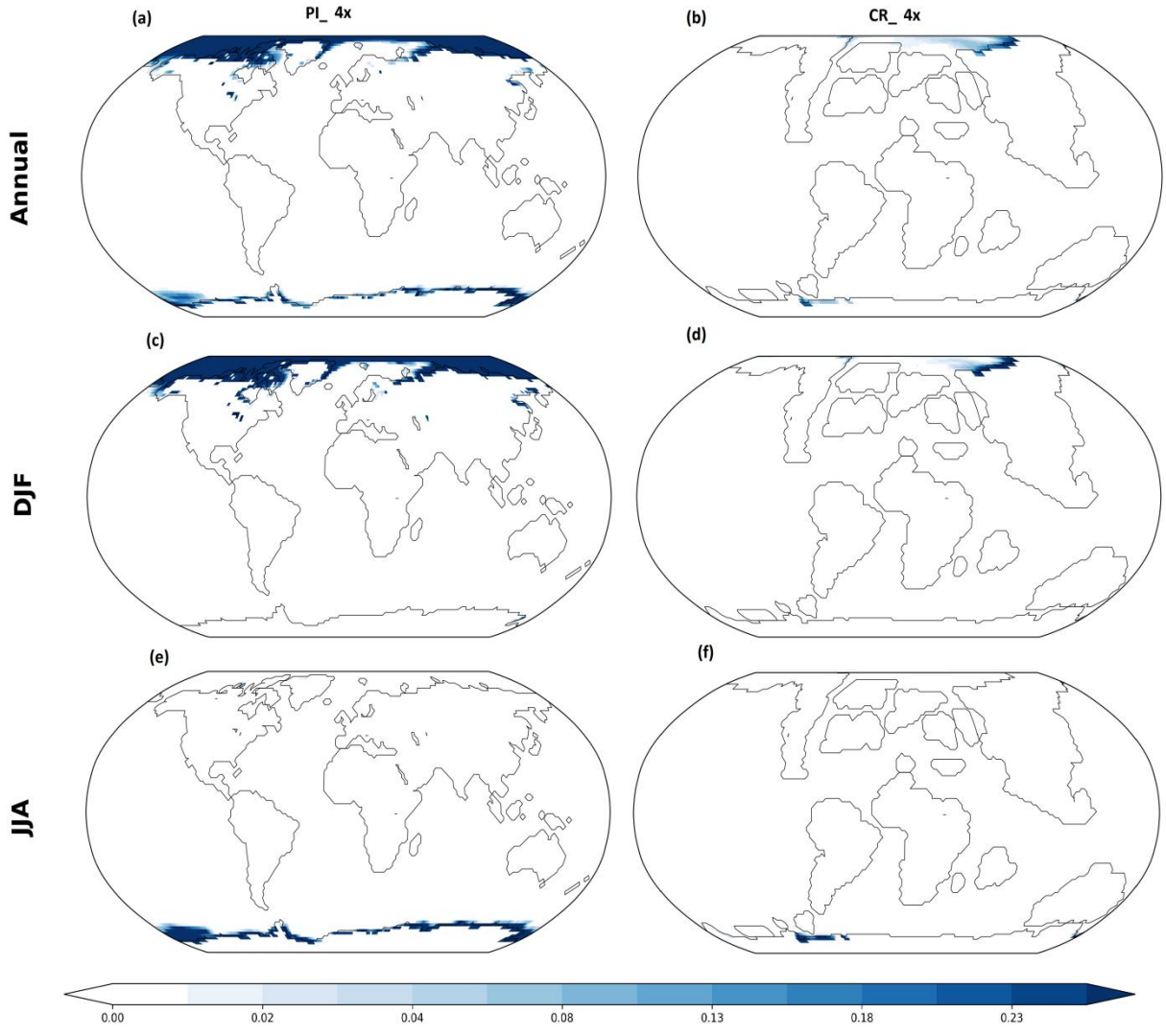

Figure 4.19: Comparison between seaice of the PI and mid-Cretaceous Climate depicted for annual and seasonal mean of PI_4x and CR_4x. (a, b) is the annual mean (c,d) is the winter and (e, f) is summer.

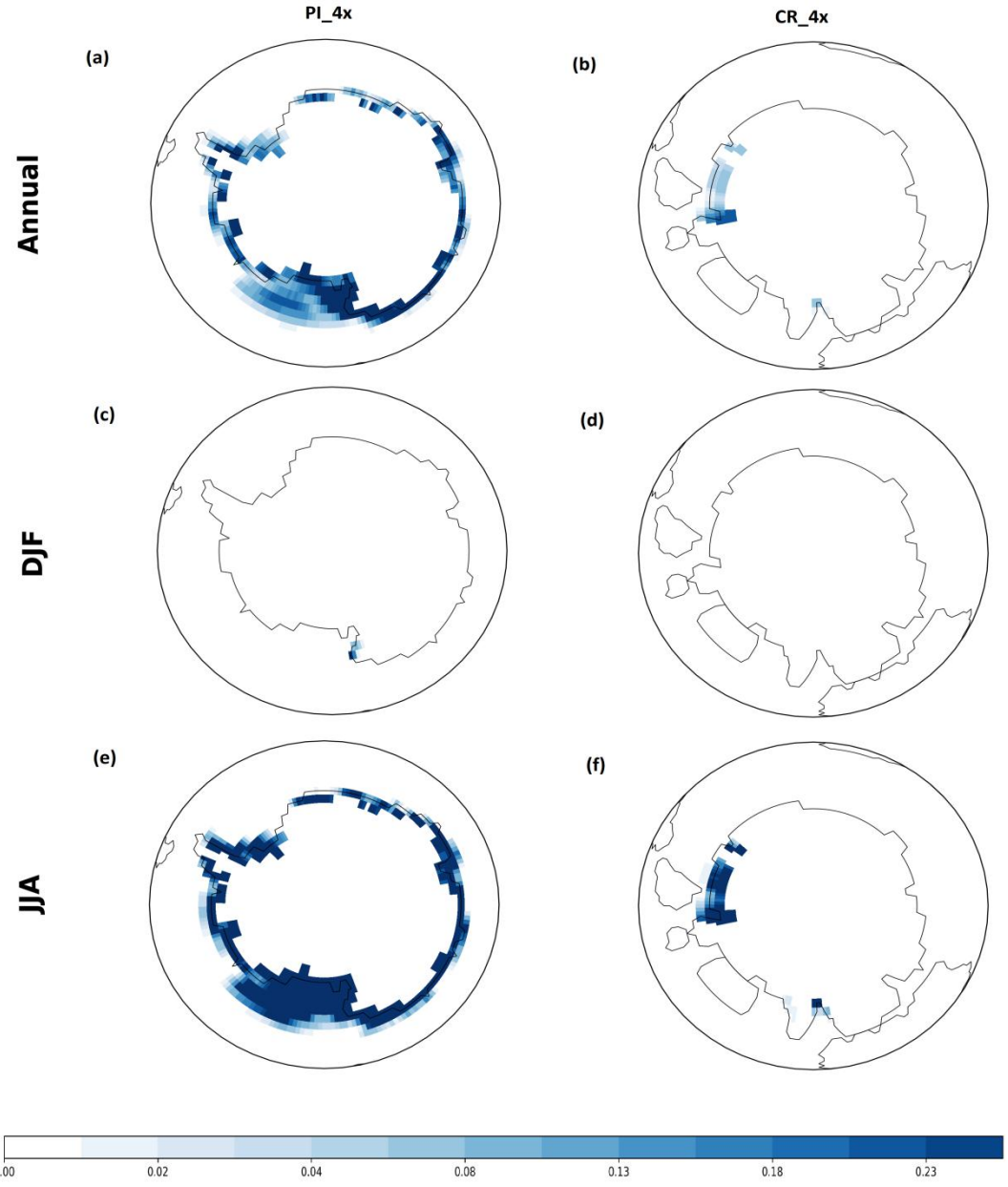

Figure 4.20: Comparison between Antarctic seaice of the PI and mid-Cretaceous Climate depicted for annual and seasonal mean of PI_4x and CR_4x. (a, b) is the annual mean (c,d) is the winter and (e, f) is summer.

4.2.3 Precipitation

The simulated precipitation anomalies (sum over convective and large-scale rainfall) of PI and mid-Cretaceous experiment with CO_2 forcing of 1,120 ppmv relative to 280 ppmv is shown in Fig 4.24. The anomalies of mean annual, boreal winter (DJF) and boreal winter (JJA) are considered. Over North America, there is an increased precipitation in the westernmost part of the PI experiment while the Cretaceous has a dipole of increased precipitation in the North-western part of the North American continent and a reduced rainfall in the mid-west. In the South America, there is also a dipole of increased precipitation in the North to mid-South America during the Cretaceous simulation with a pronounced boreal winter precipitation in the PI run. There is also a strong monsoon over India in the PI summer. In contrast to other continents, for the PI experiment, there was no sign of precipitation on Antarctica in the PI while Cretaceous on the other hand displays a slight rainfall presence in the Austral summer.

Despite the same level of CO_2 forcing in the compared PI and mid-Cretaceous simulations, there's more decrease in precipitation anomalies during the Cretaceous period than the PI, especially in the mid to high latitude. Also, the tropical region of both time periods exhibited a high precipitation sensitivity, where the Inter-tropical Convergence Zone (ITCZ) shifted slightly northward during the JJA season of both experiments. The observed mid-Cretaceous to PI precipitation difference can also be attributed to changes in vegetation types and geography of the time periods, with a higher topical land to ocean area in the Cretaceous.

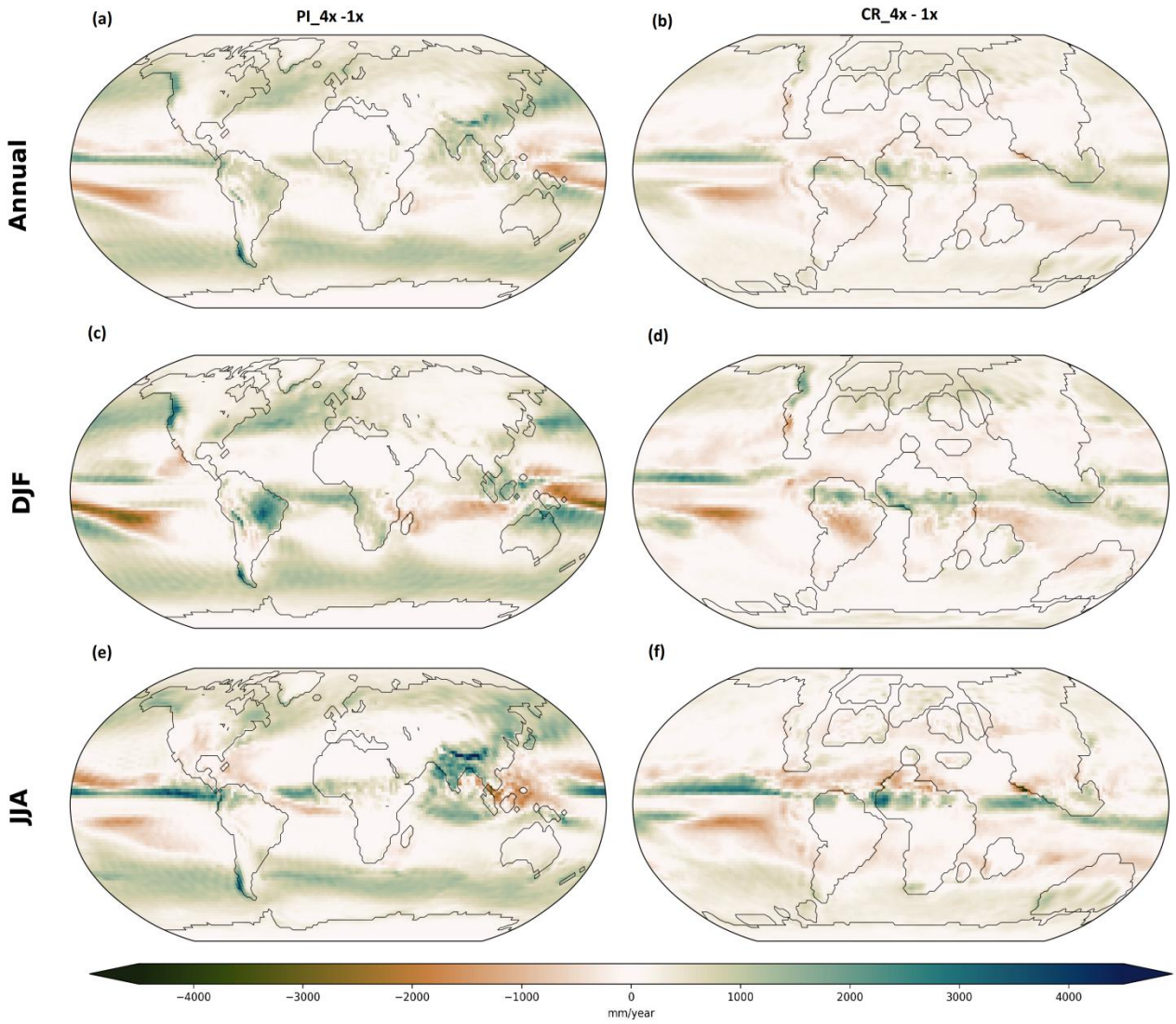

Figure 4.21: Comparison between simulated Precipitation anomalies of the PI and mid-Cretaceous climate depicted for the CO_2 values of 1,120 ppmv relative to 280 ppmv. (a,b) is annual mean, (c,d) is the winter mean and (e, f) is the summer mean. Units are mm/year.

4.3 Cretaceous Vegetation-Climate Interaction

Here, the vegetation distribution resulting from the AWI-ESM-2 mid-Cretaceous climate simulations are presented. Figures 4.22, 4.23 and 2.44 represent the spatial distribution of fractions of each pixel of the eleven plant functional types in the simulated experiments CR_1x, CR_4x, CR_6x, respectively. All three simulations were performed using the same boundary conditions and initialized with tundra-dominated vegetation. Hence, they only differ in the concentration of atmospheric carbon dioxide described in chapter 3. In the CR_1x experiment, the tropics, subtropics, mid-latitudes and high latitudes are dominated by rainforests, coniferous deciduous trees, extra-tropical evergreen trees and coniferous evergreen trees. The two other Cretaceous experiments with higher CO_2 values (CR_4x and CR_6x) still have the rainforest as the dominant plant type in the tropics while the coverage of extra-tropical evergreen trees migrates up to higher latitudes, thus making the Arctic and Antarctic dominated by a mix of coniferous evergreen trees and extra-tropical evergreen trees. The subtropics and mid-latitude of CR_4x and CR_6x are both composed of extra-tropical deciduous trees and coniferous deciduous trees.

Changes in vegetation distribution are related to changes in surface temperatures, a map of the distribution of dominant Plant Functional Types (PFTs) with corresponding surface temperature in the Antarctic is presented in Figure 4.25. The result reveal three dominant PFTs (extra-tropical evergreen trees, coniferous evergreen trees, extra-tropical deciduous trees) on the Antarctic continent. The three plant types are further presented in terms of the vegetation cover in percentage (%) (Figure 4.28).

In the CR_1x experiment, an atmospheric CO_2 concentration of 280ppmv led to warming between 0 to 10°C with West Antarctica being the coolest and East Antarctica to Australia being the warmest part covered to 80% by coniferous evergreen trees of up to 80% including some coverage of extra-tropical deciduous trees in West Antarctica and extra-tropical evergreen trees in Australia.

In case of the two high CO_2 experiments (CR_4x and CR_6x) there is an increased warming ranging from ~5 to ~ 23°C and ~10 to ~27°C in the CR_6x experiment, the large increase in

temperature in the high CO_2 experiments provides a sufficient condition for both extra-tropical evergreen trees and coniferous evergreen trees to thrive in Antarctica. Each of both PFTs cover about 50% of Antarctica while extra-tropical deciduous tree cover is only present in small areas of the continent.

4.3.2 Warmest Monthly Mean and Zonal Mean

Figure 4.26 shows the zonally averaged surface temperature (°C) for PI_1x and PI_4x in three mid-Cretaceous simulations. At Southern high latitudes, all mid-Cretaceous experiments yield significantly high zonal average surface temperature than the PI experiments. The zonal surface temperatures in the Southern high latitude increases simultaneously to the CO_2 values in both time periods. However, both CR_1x and PI_1x show similar level of zonal surface temperature most especially in the southern mid to low latitude while other three experiments exhibits increase in zonal surface temperature with increased CO_2 concentration in the order PI_4x, CR_4x, and CR_6x. Overall, zonal surface temperature peaks in the low latitude for all simulations while the lowest temperature observed for all in the high latitudes, particularly high Southern latitudes. There is a lower temperature gradient in the high CO_2 mid-Cretaceous experiments than the PI, and the CR_4x and CR_6x exhibits a zonal average temperature above freezing in Antarctica (~76°S) and the Arctic (~80°N). Remarkable differences between the mid-Cretaceous and PI experiments can be explained by higher greenhouse gas concentrations, lower ice albedo feedback, reduced elevation resulting from Greenland and Antarctic ice sheet absence (Oglesby, 1989), as well as changes in ocean currents and a more southward location of continents in the Cretaceous palaeogeography. The proxy-based temperature reconstruction mostly match with the simulated CR_4x and CR_6x.

The warmest monthly mean mid-Cretaceous surface temperature is presented in figure 4.27, unlike the zonal mean, the WMMT infers warming from the equator to south pole, with a much lower equator to pole temperature gradient. There is about 7°C drop in the WWMT between 74°S and 50°S for each of the mid-Cretaceous simulations. The low latitude (~18°S) experienced the warmest temperature, an average of 16°C warmer than the South Pole.

The AWI-ESM-2 simulation of the Cretaceous further confirms that the summer surface temperature of about ~20˚C at 82˚S can only be recreated by employing an experiment set up with atmospheric CO_2 concentrations between four to six times the PI levels.

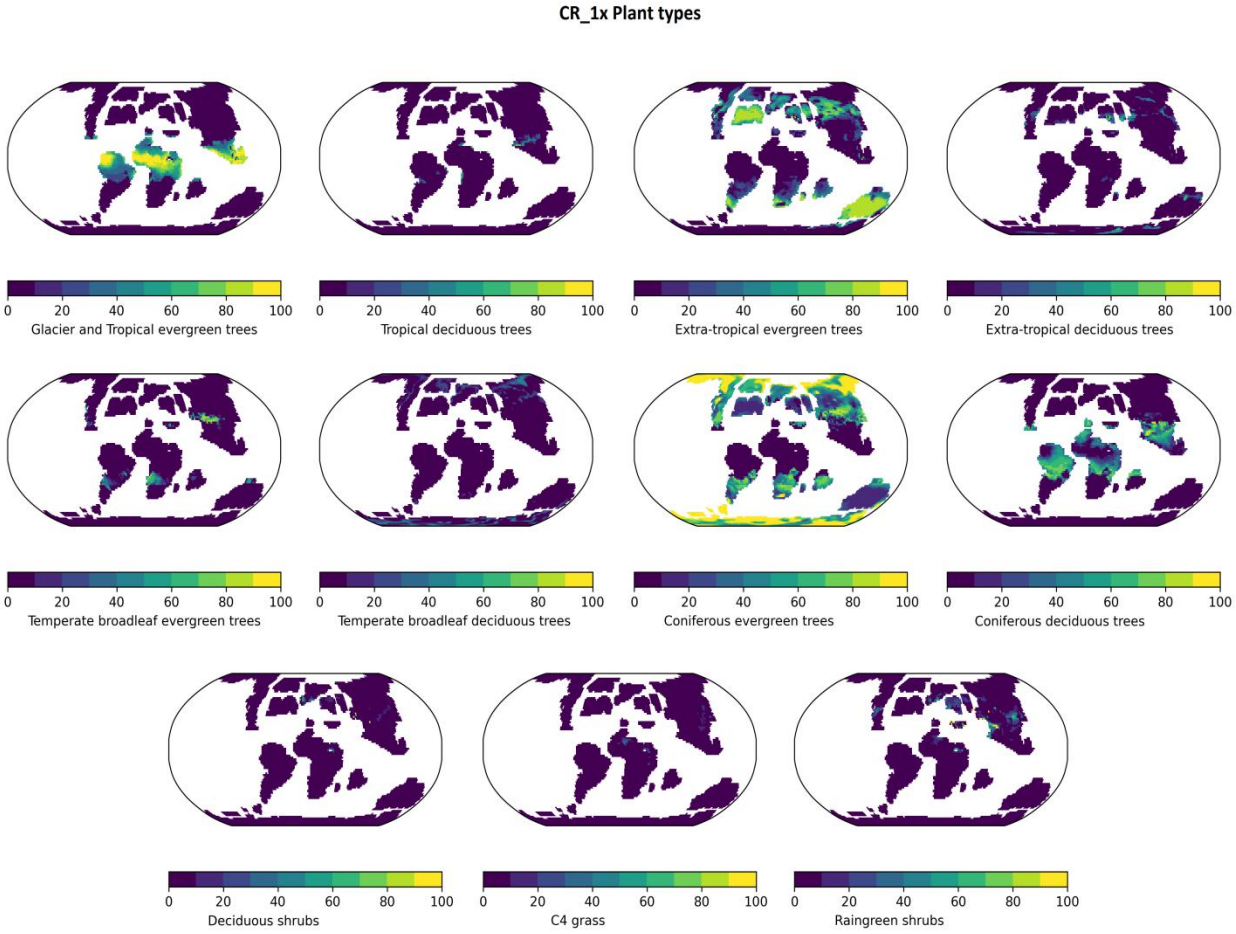

Figure 4.22: Global distribution of each plant type in the CR_1x experiment

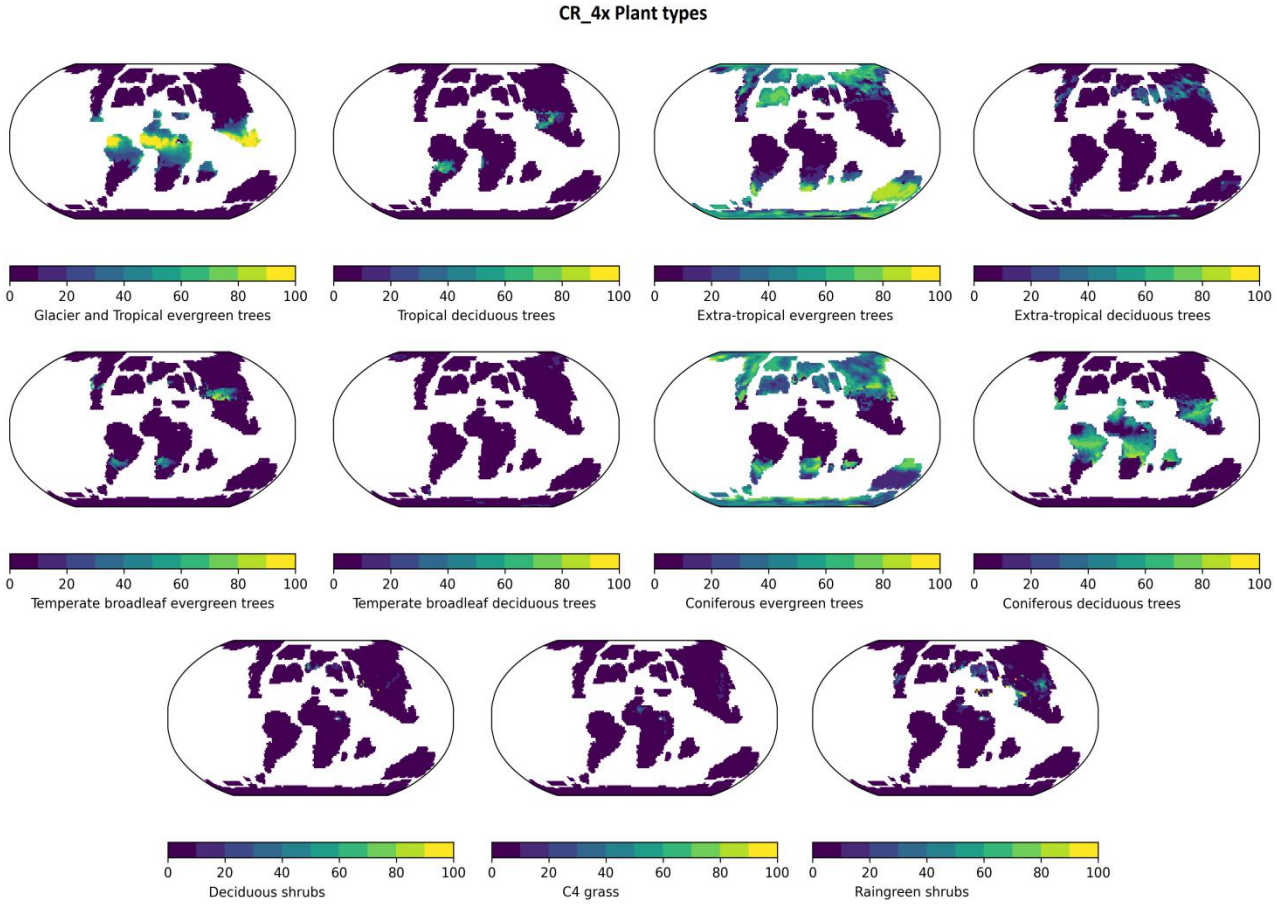

Figure 4.23: Global distribution of each plant type in the CR_4x experiment

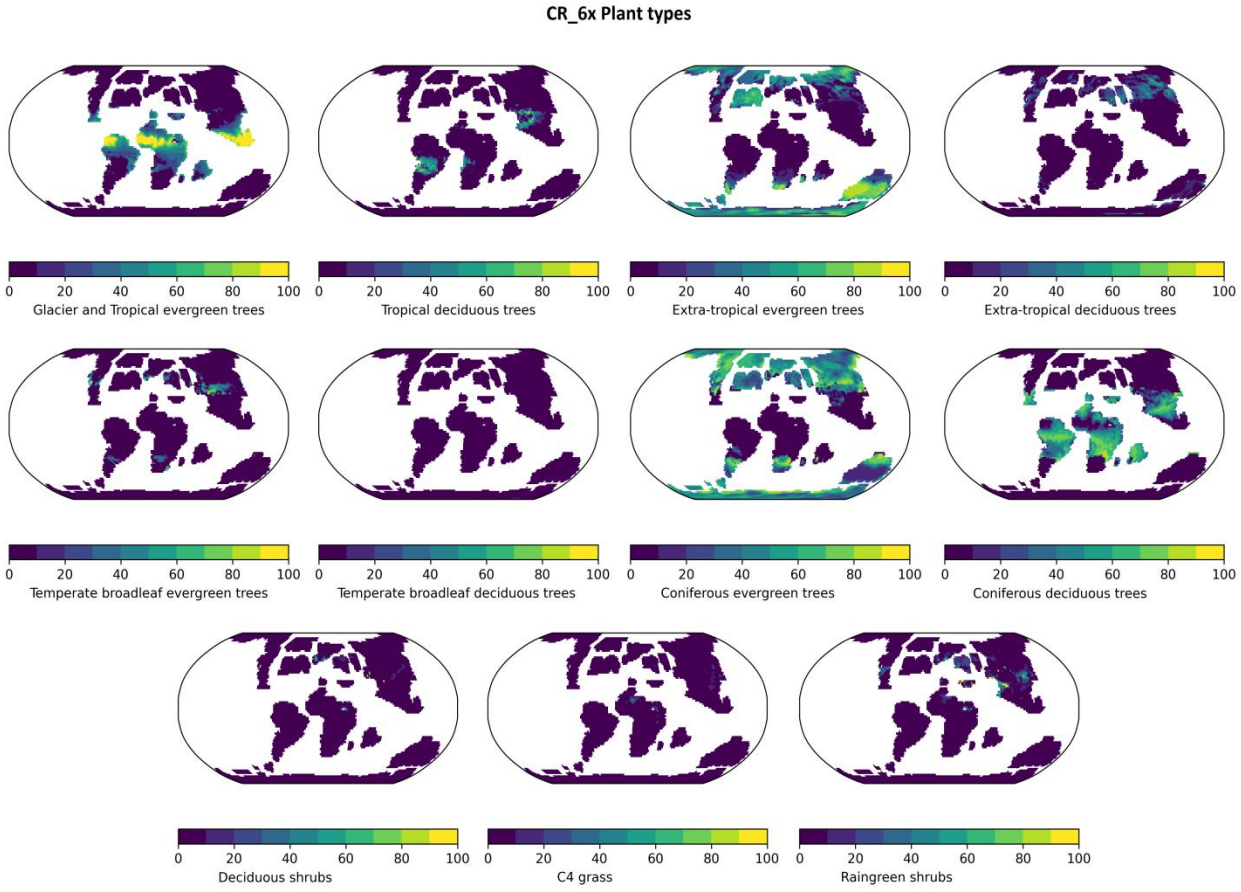

Figure 4.24: Global distribution of each plant type in the CR_6x experiment

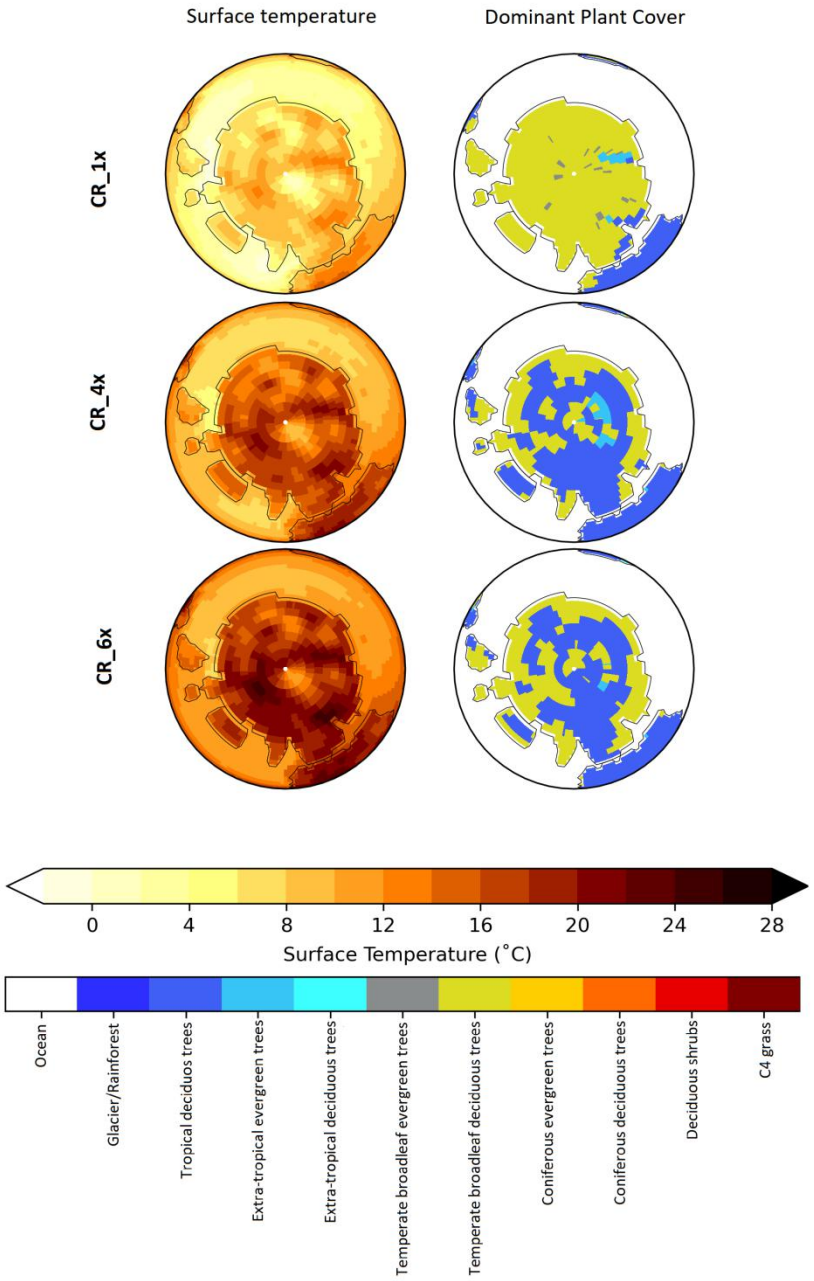

Figure 4.25: Simulated Antarctic Summer surface temperature and vegetation types of the Cretaceous

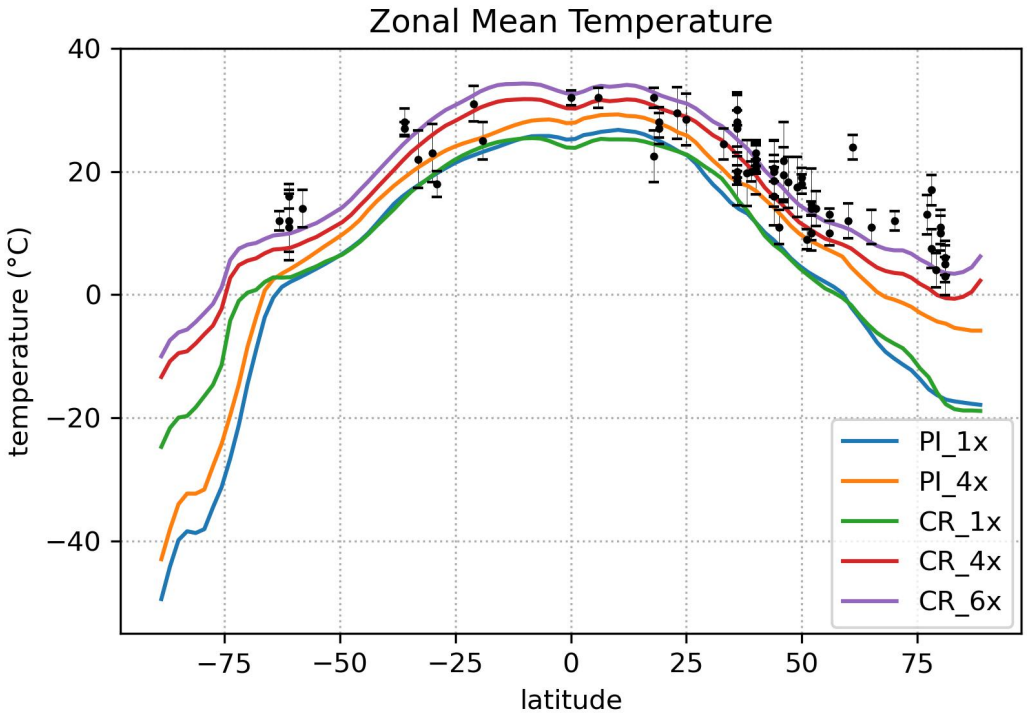

Figure 4.26: Zonal mean surface temperature and of all five simulations (Cretaceous and PI experiment). Units are ˚C.

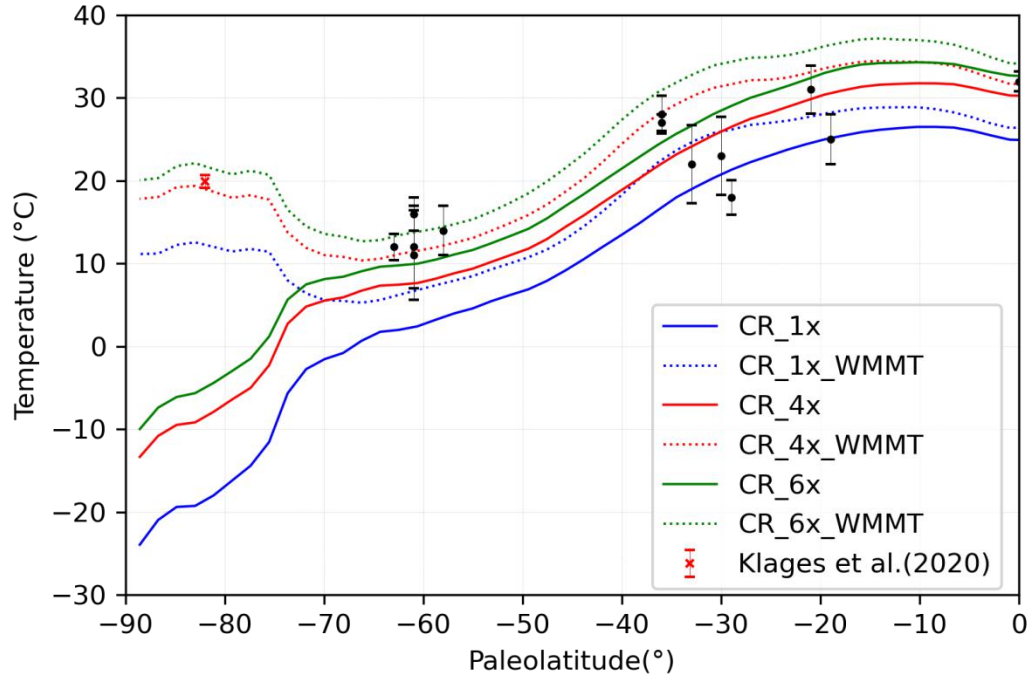

Figure 4.27: Simulated Cretaceous WMMT(dashed lines) and Zonal mean temperatures (solid line) for CR_1x, CR_4x and CR_6x experiments. Units are ˚C.

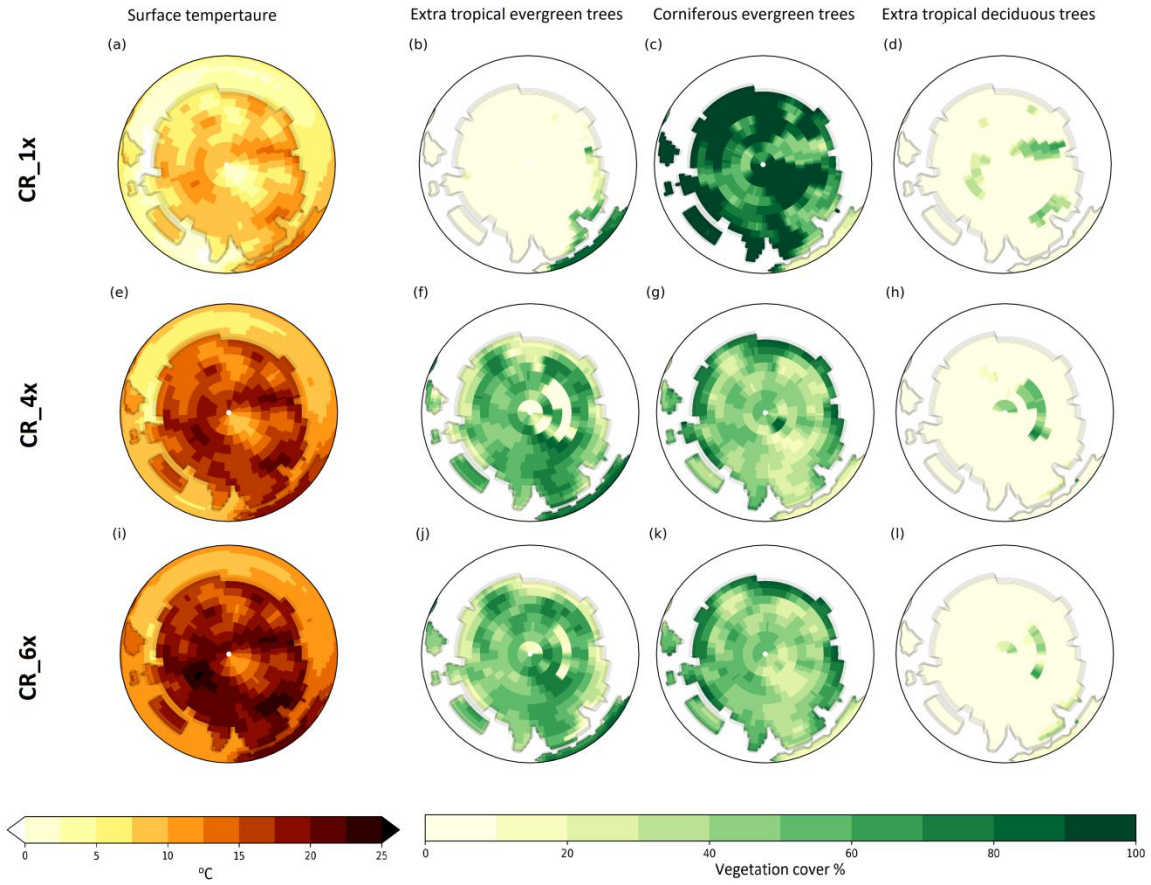

Figure 4.28: Simulated Cretaceous Summer surface temperature and the three dominant vegetation types.

CHAPTER 5

Conclusion and Outlook

The aim of this master thesis was to investigate the sensitivity of the mid-Cretaceous climate to different CO_2 forcing using the AWI-ESM-2, a coupled atmosphere-ocean-land model with interactive vegetation.The thesis applies this newly developed model for simulating deep time climates for the first time.

The simulated mid-Cretaceous climate with different CO_2 concentrations suggests that surface temperature increased simultaneously to the level of CO_2, with about 7°C increase between a 4x PI CO_2 scenario and 1x PI CO_2 (and another, ~3°C increase in the CR_6x run). The surface temperature is more affected by the CO_2 forcing particularly in high latitudes at different seasons, with the Antarctic warming to levels as high as ~23°C in the Southern summer during a 6x PI CO_2 scenario. This is close to the findings of Klages et al., (2020), stating that summer surface air and water temperature of ~20°C at about 82° South. Such values can only be simulated by forcing the climate with atmospheric CO_2 concentration of 4x to 6x PI levels. In contrast, higher CO_2 levels led to more melting, with the ice cover almost absent in the 6x PI CO_2 scenario. In the 1x PI simulation, ice cover is prominently present in Arctic Ocean in both winter and summer. Unlike the sea ice, a ~0.25 m thick snow cover exists only during the Austral and Boreal winter, indicating seasonal dependency. Hence, under a greenhouse climate simulated for CR_4x and CR_6x, permanent ice masses cannot survive on the Antarctic continent.

The results also suggest more wetness in the tropics during the summer months, as well as in South East Asia and the North Pacific, likely indicating a monsoonal condition in the region. Precipitation on the Antarctic continent appears to be unaffected by changing CO_2 concentrations since no significant precipitation changes can be observed.

This study corroborates previous studies (Klages et al., 2020) as it concludes that atmospheric CO_2 contents of at least 1120 ppmv need to be met for maintaining reconstructed vegetation during peak Cretaceous warmth. A comparison of the PI and mid-Cretaceous simulation shows that the CR_4x experiment has an average surface temperature much warmer than the PI_4x especially towards the South Pole. Implying that even under the same level of atmospheric CO_2, the mid-Cretaceous climate could still be warmer than a possible quadrupled level of PI CO_2 with the present geography.

The coupled atmosphere-ocean-land with interactive vegetation approach in simulating the mid-Cretaceous climate confirms the influence of significant feedbacks, particularly over an ice-free Antarctic continent. The Antarctic mid-Cretaceous terrestrial ecosystem seems to be sensitive to changes in the atmospheric CO_2 by shifting from dominant coniferous evergreen forests in the CR_1x experiment towards extra-tropical evergreen forest in the 4x and 6x PI runs. Thus, Antarctica was dominated by a mix of coniferous and extra-tropical evergreen trees under such high CO_2 scenarios.

This study confirms the ability of the newly developed AWI-ESM-2 to effectively simulate deeper time climates especially at high latitudes, it thus reveals high potential to more reliably estimate the magnitudes of possible future climate change, particularly in Earth's high latitude regions.

Also, the expansion of Antarctic vegetation could have contributed to Cretaceous polar warmth through reduced cloud cover and surface albedo (Zhou et al, 2012) , there could be more improvement in the climate model to include more explicit scheme for cloud feedback.

The AWI-ESM-2 can be used to simulate the mid-Cretaceous climate but without interactive vegetation and then compared to this study to quantify the role of the vegetation in the Cretaceous warmth simulated in this thesis. In addition the results from this study can also be compared to others or future coupled atmosphere-ocean models with interactive vegetation in order to estimate probable model bias.

Acronyms

AWI-CM: Alfred Wegener Institute Climate Model

AWI-ESM: Alfred Wegener Institute - Earth System Model

CDO: Climate Data Operator

COSMOS: Community Earth System Models

DJF: December–January–February

ECHAM: European Centre Hamburg Model

FESOM: Finite-Element Sea Ice–Ocean Model

GHGs: Green-House Gases

IPCC: Intergovernmental Panel on Climate Change (IPCC)

JJA: June–July–August

MPI-M: Max Planck Institute for Meteorology

NetCDF: Network Common Data Form

PI: Pre-Industrial

References

Baines, P. G. & Palmer, T. N. (1990). Rationale for a new physically-based parametrization of subgrid-scale orographic effects. *European Centre for Medium-Range Weather Forecasts, 169,* 7875-7886.

Barney, L. (2016). AWI Uses New Cray Cluster for Earth Sciences and Bioinformatics. Retrieved from *https://www.hpcwire.com/awi-uses-new-cray-cluster-earth-sciencesbioinformatics.html,* 12/22/16.

Barron, E. J. (1983) A warm equable Cretaceous: The nature of the problem. *Earth Science Reviews, 19*, 305-338.

Barron, E.J., & Washington, W.M. (1984). The role of geographic variables in explaining paleoclimates: Results from Cretaceous climate model sensitivity studies. *Journal of Geophysical Research, 89*, 1267-1279.

Berner, R. A. (1997). The rise of plants and their effect on weathering and atmospheric $C0_2$. *Scien*ce, *276*(5312), 544-546.

Brierley, C. M., Zhao, A., Harrison, S. P., Braconnot, P., Williams, C. J. R., Thornalley, D. J. R., …. Abe-Ouchi, A. (2020). Large-scale features and evaluation of the PMIP4-CMIP6 mid-holocene simulations. *Climate of the Past, 16*(5), 1847-1872.

Danilov, S., Wang, Q., Timmermann, R., Iakovlev, N., Sidorenko, D. , Kimmritz, M. , … Schröter, J. (2015). Finite-Element Sea Ice Model (FESIM). *Geoscientific Model Development, 8*, 1747-1761.

Danilov, S., Sidorenko, D., Wang, Q., & Jung, T. (2017). The Finite-volume sea ice-Ocean Model (FESOM2). *Geoscientific Model Development, 10*(2), 765-789.

DeConto, R. M. (1996). *Late Cretaceous climate, vegetation and ocean interactions, An Earth system approach to modelling an extreme climate.* Ph.D. thesis, University of Colorado, Boulder, CO.

DeConto, R. M., Brady, E. C., Bergengren, J., and Hay, H. H. (2000). *Late Cretaceous Climate, Vegetation, and Ocean Interactions*, in: Warm Climates in Earth History, edited by: Huber, B., MacLeod, K. G., and Wing, S. L., Cambridge University Press, 275–297.

Edwards, P. N. (2011) *A Vast Machine: Computer Models, Climate Data, and the Politics of Global Warming.* Cambridge, MA: MIT Press.

Francis, J. E., Ashworth, A., Cantrill, D. J., Crame, J. A., Howe, J., Stephens, … Thorn, V. (2007). 100 million years of Antarctic Climate Evolution: Evidence from fossil plants. *Open-File Report*, 19–28. https://doi.org/10.3133/ofr20071047kp03

Gierz, P., Ackermann, L., Rodehacke, C. B., Krebs-Kanzow, U., Stepanek, C., Barbi. D., & Lohmann, G. (2020). Simulating interactive ice sheets in the multi-resolution AWI-ESM-1.2: A case study using SCOPE 1.0. *Geoscientific Model Development.* Discuss. [preprint], https://doi.org/10.5194/gmd-2020-159, 2020.

Giorgetta, M. A., Jungclaus J., Reick, C. H., Legutke, S., Bader, J., Böttinger, M., … Stevens, B. (2013). Climate and carbon cycle changes from 1850 to 2100 in MPI-ESM simulations for the Coupled Model Intercomparison Project Phase 5. *Journal of Advances in Modeling Earth Systems, 5*(3) 572-597.

Haid, V., & Timmermann, R. (2013). Simulated heat flux and sea ice production at coastal polynyas in the south-western Wed-dell Sea. *Journal of Geophysical Research: Oceans*, *118*(5), 2640-2652.

Haid, V., Timmermann, R., Ebner, L., & Heinemann, G. (2015). Atmospheric forcing of coastal polynyas in the south-western Wed-dell Sea. *Antarctic Science*, *27*(4), 388-402.

Hannah, E. D. (2015). Comparing results of global integrated assessment models. *Environmental Scieince and Technology, 49*(17), 10701-10709.

Hay, W. W. (2011). Can humans force a return to a "Cretaceous" climate?. *Sedimentary Geology, 235*(1-2), 5-26.

Hellmer, H. H., Kauker, F., Timmermann, R., Determann, J., & Rae, J. (2012). Twenty-first-century warming of a large Antarctic ice-shelf cavity by a redirected coastal current. *Nature*, *485*(7397), 225–228. https://doi.org/10.1038/nature11064

Higuchi, T., Abe-Ouchi, A., Chan, W. (2021). Differences between present-day and mid-Cretaceous hydrological cycle responses to rising CO_2 concentration. *Geophysical Research Letters, 48*(22).

Hurtt, G. C., Chini, L. P., Frolking, S., Betts, R. A., Feddema, J., Fischer, G., … Wang, Y. P. (2011). Harmonization of land-use scenarios for the period 1500–2100: 600 years of global gridded annual land-use transitions, wood harvest, and resulting secondary lands. *Climatic Change*, *109*(1-2), 117–161. https://doi.org/10.1007/s10584-011-0153-2

International Chronostratigraphic Chart. (n.d.). Retrieved January 1, 2022, from https://stratigraphy.org/ICSchart/ChronostratChart2021-10.pdf

Karl, T. R. & Trenberth K. E. (2003). Modern global climate change. *Science. 302,* 1719-1723.

Kageyama, M., Harrison, S. P., Kapsch, M.-L., Löfverström, M., Lora, J. M., Mikolajewicz, U., … Volodin, E. (2020a). The PMIP4-CMIP6 last glacial maximum experiments: preliminary results and comparison with the PMIP3-CMIP5 simulations. *Climate of the Past Discussions*, in review.

Kageyama, M., Sime, L. C., Sicard, M., Guarino, M.-V., de Vernal, A., Schroeder, D., … Ziehn, T., (2020b). A multi-model CMIP6 study of Arctic sea ice at 127 ka: Sea ice data compilation and model differences. *Climate of the Past Discussions*, accepted.

Kinne, S., O´Donnel, D., Stier, P., Kloster, S., Zhang, K., Schmidt, H., … Stevens, B. (2013). MAC-v1: A new global aerosol climatology for climate studies. *Journal of Advances in Modelling Earth System, 5*(4), 704-740.

Klages, J.P., Salzmann, U., Bickert, T., Hillenbrand, C., Gohl, K., Kuhn, G., … Science Team of Expedition of PS104. (2020). Temperature rainforests near the South Pole during peak Cretaceous warmth. *Nature, 580*, 81-86.

Knorr, G., & Lohmann, G. (2014). Climate warming during Antarctic ice sheet expansion at the Middle Miocene transition. *Nature Geoscience, 7,* 376-381.

Knorr, G., Butzin, M., Michaels, A., & Lohmann, G. (2011). A warm Miocene climate at low atmosphere CO_2 levels. *Geophysical Research Letters,* 38 (20).

Laskar, J., Robutel, P., Joutel, F., Gastineau, M., Correia, A.C.M., & Levrard, B. (2004). A long-term numerical solution for the insolation quantities of the Earth. *Astronomy and Astrophysics, 428*(1), 261-285. //doi.org/10.1051/0004-6361:20041335.

Lohmann, G., Butzin, M., Eissner, N., Shi, X., & Stepanek, C. (2020). Abrupt climate and weather changes across timescales. *Paleoceanography and Paleoclimatology*, *35,* e2019PA003782.

Markwick, P.J. (2007). The palaeogeographic and palaeoclimatic significance of climate proxies for data-model comparisons, deep-time perspectives on climate change: Marrying the signal from computer models and biological proxies. *The Geological Society*, 251-312.

Markwick, P. J. & Valdes, P. J. (2004). Palaeo-digital elevation models for use as boundary conditions in coupled ocean-atmosphere GCM experiments: a Maastrichtian (late Cretaceous) example. *Palaeogeography, Palaeoclimatology, Palaeoecology, 213*(1-2) 37-63.

Miller, K. G., Kominz, M. A., Browning, J. V., Wright, J. D., Mountain, G. S., Katz, M. E., … Pekar, S. F. (2005). The Phanerozoic record of sea-level change. *Science, 310*, 1293-1298.

Müller, R. D., Sdrolias, M., Gaina, C., Steinberger, B., & Heine, C. (2008). Long-Term Sea-Level Fluctuations Driven by Ocean Basin Dynamics. *Science, 319,* 1357-1362.

Niezgodzki, I., Knorr, G., Lohmann,G., Tyszka, J., & Markwick, P. J. (2017). Late Cretaceous climate simulations with different CO_2 levels and subarctic gateway configuration: A model-data comparison. *Paleoceanography, 32*(9), 980-998.

Oglesby, R. J. (1989). A GCM study of Antarctic Glaciation, *Climate Dynamics*, *3,* 135–156.

Otto-Bliesner, B.L., Brady, E.C., & Shields, C. (2002). Late Cretaceous ocean: Coupled simulations with the national center for atmospheric research climate system model. *Journal of Geophysical Research: Atmosphere, 107*(D2) 11-14.

Otto-Bliesner, B.L. & Brady, E.C. (2001). Tropical pacific variability in the NCAR climate system model. *Journal of Climate, 14*(17) 3587-3607.

Otto-Bliesner, B. L., Brady, E. C., Zhao, A., Brierley, C., Axford, Y., Capron, E., … Zheng, W. (2020). Large-scale features of Last Interglacial climate: Results from evaluating the lig127k simulations for CMIP6-PMIP4. *Climate of the Past Discussions*, accepted.

Perlmutter-powered deep-learning model speeds extreme weather predictions. HPCwire. (2016, November 30). Retrieved December 12, 2021, from https://www.hpcwire.com/off-the-wire/perlmutter-powered-deep-learning-model-speeds-extreme-weather-predictions/.

Poole, I., Cantrill, D. J. & Utescher, T. (2005). Reconstructing Antarctic palaeoclimate from wood floras: a comparison using multivariate anatomical analysis and the coexistence approach. *Palaeogeography, Palaeoclimatology, Palaeoecology, 222*(95–121) .

Puceat, E., Donnadieu, Y., Ramstein, G., Fluteau, F., & Guillocheau, F. (2005). Numerical evidence for thermohaline circulation reversals during the Maastrichtian.*Geochemistry, Geophysics, Geosystems, 6*(11).

Rast, S., Brokopf, R., Cheedela, S. K., Esch, M., Gayler, V., Kirchner, I., ... & Wieners, K. H. (2013). User manual for ECHAM6-June 21, 2013,(2013-02-26), version echam-6.1. 06p3-guide-1.3.

Reick, C. H., Gayler, V., Goll, D., Hagemann, S., Heidkamp, M. & Nabel, J. E. M. S., (2021). JSBACH 3 - The land component of the MPI Earth System Model: documentation of version 3.2. *Hamburg: MPI for Meteorologie, 240,* 271-282.

Ramankutty, N., & Foley, J. A. (1999). Estimating historical changes in global land cover: Croplands from 1700 to 1992. *Global Bio- geochemical Cycle, 13*, 997–1027.

Richler, J. J., Tanaka, J. W., Brown, D. D., & Gauthier, I. (2008). Why does selective attention to parts fail in face processing? *Journal of Experimental Psychology: Learning, Memory, and Cognition, 34*(6), 1356–1368. https://doi.org/10.1037/a0013080

Roeckner, E., Brokopf, R., Esch, M., Giorgetta, M., Hagemann, S., Kornblueh, L., … Schulzweida, U. (2006). Sensitivity of simulated climate to Horizontal and Vertical resolution in the ECHAM5 Atmosphere Model. *Journal of Climate, 19*(16) 3771-3791.

Roeckner E., Bäuml, G., Bonaventura, L., Brokopf, R., Esch, M., Giorgetta, M., …Tompkins, A. (2003). The atmospheric general circulation model ECHAM5. PART I: model description. *Report/ Max-Planck-Institut fur Meteorologie, 349.*

Schmidt, G. A., Jungclaus, J. H., Ammann, C. M., Bard, E., Braconnot, P. , Crowley, T. J., … Vieira, L.E.A. (2012). Climate forcing reconstructions for use in PMIP simulations of the Last Millennium (v1.1). *Geoscientific Model Development, 5,* 185-191.

Scholz, P. , Kieke, D. , Lohmann, G. , Ionita, M., & Rhein, M. (2014). Evaluation of labrador sea water formation in a finite-element sea-ice ocean model setup, based on a comparison with observational data. *Journal of Geophysical Research - Oceans, 3*, 1644-1667.

Scholz P., Lohmann G., Wang Q., & Danilov, S. (2013). Evaluation of a Finite-Element Sea-Ice Ocean Model (FESOM) set-up to study the inter-annual to decadal variability in the deep-water formation rates. *Ocean Dynamics, 63*(4), 347-370.

Schulzweida, U. (2019). CDO User Guide (Version 1.9.8). Zenodo. http://doi.org/10.5281/zenodo.3539275.

Sewall, J. O., van de Wal, R.S.W., van der Zwan, K., van Osterhout, C., Dijkstra, H.A., & Scotese, C.R. (2007). Climate model boundary conditions for four Cretaceous time slices.*Climate of the Past, 3*(4) 647 - 657.

Shellito, J., Sloan, C., & Huber M. (2003), Climate model sensitivity to atmospheric CO_2 levels in the Early-Middle Paleogene. *Paleogeography, Paleoclimatology, Palaeoecology, 193*(1) 113-123.

Sein, D. V., Koldunov, N. V., Danilov, S., Sidorenko, D., Wekerle, C., Cabos, W., … Jung T., 2018. The relative influence of atmospheric and oceanic model resolution on the circulation of the North Atlantic Ocean in a coupled climate model. *Journal in Advances in Modeling Earth Systems*, *10*(8), 2026-2041.

Sidorenko, D., Rackow, T., Jung, T., Semmler, T., Barbi ,D., Danilov, S., … Wang, Q. (2015). Towards multi-resolution global climate modeling with ECHAM6–FESOM. Part I: model formulation and mean climate. *Climate Dynamics*, *44*(3-4), 757-780.

Sidorenko, D., Goessling, H. F., Koldunov, N. V., Scholz, N. P., Danilov, S., Barbi, D., … Jung , T. (2019). Evaluation of FESOM2.0 coupled to ECHAM6.3: PI and HighResMIP smulations. *Journal of Advances in Modelling Earth Systems, 11*(11), 3794-3815.

Sloan, L.C. & Barron, E. J. (1990). "Equable" climate during Earth history? *Geology*, 489-492.

Shi, X., Yang, H., Danek, C. & Lohmann, G. (2020). AWI AWI-ESM1.1LR model output prepared for CMIP6 PMIP lgm. *Earth System Grid Federation*. doi.org/10.22033/ESGF/CMIP6.9330

Starz, M., Lohmann, G., & Knorr, G. (2016). The effect of a dynamic soil scheme on the climate of the mid-Holocene and the Last Glacial Maximum. *Climate of the Past, 12*(1) 151-170.

Stenchikov, G. L., Kirchner, I., Robock, A., Graf, H., Antuña, J.C., Grainger,R. G., … Thomason, L. (1998). Radiative forcing from the 1991 Mount Pinatubo volcanic eruption. *Journal of Geophysical Research, 103*(D12),13837-13857.

Stepanek C. & Lohmann G. (2012). Modelling Mid-Pilocene climate with COSMOS. *Geoscientific Model Development, 5*(5), 1221-1243.

Stevens, B., Giorgetta, M., Esch, M., Mauritsen, T., Crueger, T., Rast, S., ... & Roeckner, E. (2013). Atmospheric component of the MPI-M Earth system model: ECHAM6. *Journal of Advances in Modeling Earth Systems*, *5*(2), 146-172.

Upchurh, G.R., Kiehl, J., Shields, C., Scherer, J., & Scotese, C. (2015). Latitudinal temperature gradients and high-latitude temperatures during the latest Cretaceous: Congruence of geologic data and climate models. *Geology, 43*(8), 683-686.

Valdes, P. J., Sellwood, B. W. & Price, G. D. (1996). Evaluating concepts of Cretaceous equability. *Paleoclimates, 2*, 139-158.

Wekerle, C., Wang, Q., Danilov, S., Jung, T., & Schröter, J. (2013). The Canadian Arctic Archipelago throughflow in a multiresolution global model: Model assessment and the driving mechanism of interannual variability. *Journal of Geophysical Research: Oceans*, *118*(9), 4525-4541.

Winguth, A., Shellito, C., Shields, C., & Winguth, C. (2010). Climate response at the paleocene-eocene thermal maximum to greenhouse gas forcing – A Model Study with CCSM3. *Journal of Climate, 23*(10) 2562-2584.

Zhou, J., Poulsen, C. J., Rosenbloom, N., Shields, C., & Briegleb, B. (2012). Vegetation-climate interactions in the warm mid-Cretaceous. *Climate of the past, 8,* 565-576.